

AWARD NUMBER: **W81XWH-13-1-0086**

TITLE: **Circumventing Therapeutic Resistance and the Emergence of Disseminated Breast Cancer Cells Through Non-Invasive Optical Imaging**

PRINCIPAL INVESTIGATORS: **Michael J. Therien**

CONTRACTING ORGANIZATION: **Duke University**  
Durham, NC 27705-4677

REPORT DATE: **June 2015**

TYPE OF REPORT: **Annual**

PREPARED FOR: U.S. Army Medical Research and Materiel Command  
Fort Detrick, Maryland 21702-5012

DISTRIBUTION STATEMENT: Approved for Public Release;  
Distribution Unlimited

The views, opinions and/or findings contained in this report are those of the author(s) and should not be construed as an official Department of the Army position, policy or decision unless so designated by other documentation.

<b>REPORT DOCUMENTATION PAGE</b>				<i>Form Approved</i> <i>OMB No. 0704-0188</i>	
Public reporting burden for this collection of information is estimated to average 1 hour per response, including the time for reviewing instructions, searching existing data sources, gathering and maintaining the data needed, and completing and reviewing this collection of information. Send comments regarding this burden estimate or any other aspect of this collection of information, including suggestions for reducing this burden to Department of Defense, Washington Headquarters Services, Directorate for Information Operations and Reports (0704-0188), 1215 Jefferson Davis Highway, Suite 1204, Arlington, VA 22202-4302. Respondents should be aware that notwithstanding any other provision of law, no person shall be subject to any penalty for failing to comply with a collection of information if it does not display a currently valid OMB control number. <b>PLEASE DO NOT RETURN YOUR FORM TO THE ABOVE ADDRESS.</b>					
<b>1. REPORT DATE</b> June 2015		<b>2. REPORT TYPE</b> Annual		<b>3. DATES COVERED</b> 1 July 2014 – 30 May 2015	
<b>4. TITLE AND SUBTITLE</b> Circumventing Therapeutic Resistance and the Emergence of Disseminated Breast Cancer Cells Through Non-Invasive Optical Imaging				<b>5a. CONTRACT NUMBER</b> W81XWH-13-1-0086	
				<b>5b. GRANT NUMBER</b>	
				<b>5c. PROGRAM ELEMENT NUMBER</b>	
<b>6. AUTHOR(S)</b> Michael J. Therien, Neil L. Spector  E-Mail: <a href="mailto:michael.therien@duke.edu">michael.therien@duke.edu</a> , <a href="mailto:neil.spector@duke.edu">neil.spector@duke.edu</a>				<b>5d. PROJECT NUMBER</b>	
				<b>5e. TASK NUMBER</b>	
				<b>5f. WORK UNIT NUMBER</b>	
<b>7. PERFORMING ORGANIZATION NAME(S) AND ADDRESS(ES)</b> Duke University 2200 W. Main Street Durham, NC 27705-4677				<b>8. PERFORMING ORGANIZATION REPORT NUMBER</b>	
<b>9. SPONSORING / MONITORING AGENCY NAME(S) AND ADDRESS(ES)</b>  U.S. Army Medical Research and Materiel Command Fort Detrick, Maryland 21702-5012				<b>10. SPONSOR/MONITOR'S ACRONYM(S)</b>	
				<b>11. SPONSOR/MONITOR'S REPORT NUMBER(S)</b>	
<b>12. DISTRIBUTION / AVAILABILITY STATEMENT</b>  Approved for Public Release; Distribution Unlimited					
<b>13. SUPPLEMENTARY NOTES</b>					
<b>14. ABSTRACT</b>  Herein we explore a series of optically distinct near infrared emissive polymersomes (NIREPs; biodegradable polymer vesicles that manifest extraordinarily high irradiances and are ideally suited for in vivo optical imaging), each conjugated to different antibodies for the non-invasive molecular imaging of all breast cancer sites within a patient, including micrometastases. In Year 2, we have taken significant steps to optimize NIREP fabrication protocols to ensure antibodies can be reproducibly conjugated to the surface of NIREPs while preserving native antigen-recognition properties. We have developed a fluoronitrobenzoic acid (FNB) conjugation strategy, which enables us to covalently attach trastuzumab (anti-HER2 IgG) to the surface of pre-fabricated NIREPs under mild, aqueous conditions. In model experiments, we have demonstrated that covalent modification of trastuzumab does not affect HER2 recognition properties. Furthermore, we have developed a sensitive Western blot protocol for the detection of trastuzumab attached to NIREPs to allow accurate quantification of NIREP surface functionalization density. With our new protocols, we are well placed in Year 3 to generate a cocktail of antibody-functionalized NIREPs for <i>in vitro</i> and <i>in vivo</i> evaluation.					
<b>15. SUBJECT TERMS</b> Breast cancer, emissive polymersomes, near infrared fluorescence, therapeutic resistance, molecular profiling, personalized medicine, imaging, active targeting					
<b>16. SECURITY CLASSIFICATION OF:</b>			<b>17. LIMITATION OF ABSTRACT</b>  UU	<b>18. NUMBER OF PAGES</b>  43	<b>19a. NAME OF RESPONSIBLE PERSON</b> USAMRMC
<b>a. REPORT</b>  U	<b>b. ABSTRACT</b>  U	<b>c. THIS PAGE</b>  U			<b>19b. TELEPHONE NUMBER</b> (include area code)

## Table of Contents

	<u>Page</u>
1. Introduction.....	4
2. Keywords.....	4
3. Accomplishments.....	4
4. Impact.....	16
5. Changes/Problems.....	17
6. Products.....	18
7. Participants & Other Collaborating Organizations.....	19
8. Special Reporting Requirements.....	20
9. Appendices.....	20

## 1. INTRODUCTION

Breast cancer (BC) is a molecularly heterogeneous disease, which can be categorized into subtypes based on the tumor biology.<sup>1,2</sup> HER2 over-expressing cancers (HER2+) for example, account for 25–30% of diagnosed BCs and are associated with early metastasis and poor survival prognosis.<sup>3</sup> Treatments for HER2+ BCs, such as trastuzumab (Herceptin),<sup>4</sup> directly target the HER2 cell membrane receptor.<sup>5</sup> Such treatments are specific to HER2+ BCs, with no effect on other tumor subtypes e.g. estrogen receptor overexpressing cancers (ER+, luminal A subtype). Similarly, ER+ BC are treated with endocrine therapies targeting either ER directly e.g. tamoxifen,<sup>6</sup> or production of the receptor ligand (estradiol) e.g. aromatase inhibitors.<sup>7,8</sup> It is therefore crucial to molecularly profile a cancer to prescribe the correct program of treatment. Diagnosis and subsequent treatment of BC is often based on analysis of a single biopsy of a primary tumor, and the surrounding lymph nodes. However, this method is flawed in advanced stage cancers, as the molecular profile of the cancer may differ at metastatic sites and/or between metastases in different organs.<sup>9</sup> Furthermore, most advanced stage breast cancers that initially respond to targeted therapy, whether HER2+ or ER+, become resistant to treatment, generally in less than 12 months, resulting in disease progression.<sup>10,11</sup> The molecular heterogeneity of BC tumors, coupled with the diverse mechanisms and dynamic nature of therapy resistance,<sup>12–18</sup> illustrate that this method of diagnosis is insufficient to predict a tumor's response to treatment. This accounts for the mixed clinical responses to treatment observed in advanced stage BC patients, where some sites regress while others see progression. Developing effective treatment strategies for BC requires the ability to identify the molecular subtypes of each tumor site, and understand the mechanisms involved in the development of therapeutic resistance. However, obtaining biopsies from each site multiple times over the course of treatment is not practical. We proposed that near-infrared emissive polymersomes (NIREPs), a brightly emissive nanostructure, can be targeted to signature cell surface proteins to enable quantitative, non-invasive optical imaging of molecularly heterogeneous sites of BC in vivo. In this DoD 2014-2015 annual report, we provide an update on our progress to develop antibody-conjugated NIREPs capable of distinguishing between phenotypically distinct BC cells.

## 2. KEYWORDS

HER2, breast cancer, near infrared polymersomes, antibodies,

## 3. ACCOMPLISHMENTS

### 3.1 What were the major goals of the project?

Aim 1: Profile a panel of molecularly heterogeneous human breast cancer cell lines using cocktails of antibody-conjugated NIREPs (Years 1–3).

Aim 1.1: A panel of human breast cancer cell lines representing several of the molecular breast cancer subtypes will be profiled using a cocktail of Ab-NIREPs targeting key cell surface proteins that serve as therapeutic targets or predict for therapeutic resistance to existing targeted therapies used in the treatment of breast cancer.

Aim 1.2: The apoptotic effects of HER2-targeted therapies on HER2+ cell lines will be determined using a NIREP conjugated to commercially available recombinant annexin V.

Aim 1.3: Use of NIREPs to determine the effects of targeted therapies on breast cancer cell surface phenotype.

Aim 1.4: Generation of firefly luciferase expressing cells.

Aim 1.5: The level of sensitivity of Ab-NIREPs will be determined in limiting dilution studies.

Aim 2: To phenotype phenotypically diverse primary and metastatic sites of breast cancer using targeting NIR emissive polymersomes and determine their response to targeted therapies (Year 3).

The same cocktail of NIREPs validated in Aim 1 will be evaluated *in vivo*, using an immunocompromised mouse featuring either/both a HER2+ or HER2- MDA-MD-231 tumor xenograph.

### 3.2 What was accomplished under these goals?

Aim 1 (Years 1–3): Profile a panel of molecularly heterogeneous human breast cancer cell lines using cocktails of antibody-conjugated NIREPs.

*Therien Group:* In our prior work, we demonstrated that NIREPs featuring surfaces functionalized with the humanized anti-HER2 monoclonal antibody trastuzumab, were able to discriminate between HER2+ and HER2- cell lines in *in vitro* experiments (Figure 1d). The intent of this project is to extend these studies by developing a series of other antibody-conjugated NIREPs, each targeting a specific breast cancer-relevant cell surface antigen. Each unique NIREP would contain a porphyrin oligomer fluorophore to enable wavelength-based detection of cell receptor type (Figure 1a–c).

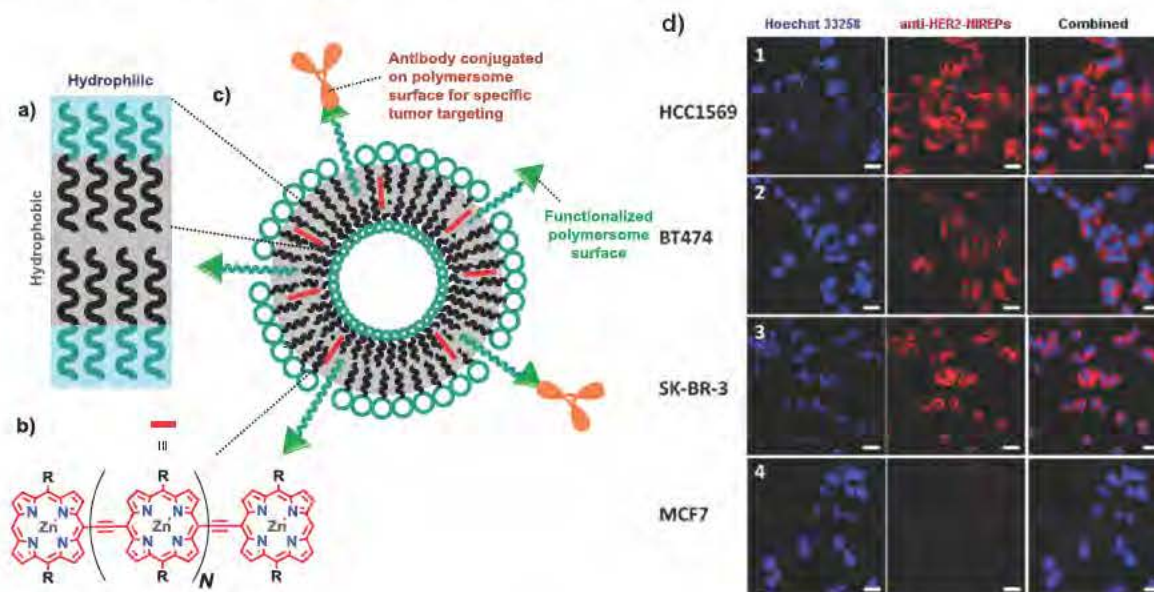


**Figure 1.** Schematic depiction of an antibody-conjugated NIREP: a) Polymersomes consist of a bilayer of amphiphiles which self-assemble in aqueous conditions. The resulting vesicle has the hydrophilic head groups pointing into the interior of the vesicle, and towards bulk solvent, with the hydrophobic chains sequestered within the membrane; b) The lipophilic membrane can be loaded with near-IR fluorophores (PZn<sub>N</sub> compounds, e.g. PZn<sub>3</sub>:  $\lambda_{\text{ex}}$  = 786 nm;  $\lambda_{\text{em}}$  = 809 nm). Number of porphyrins *N* and solubilizing groups *R* can be varied to alter emission wavelength; c) Antibody-conjugated NIREPs enable tumor specific cell targeting. (d) Anti-HER2 NIREPs can discriminate between HER2+ cells (HCC1569, BT474 and SKBR3 cells) and HER2 negative cells (MCF7). Left column: nuclei stained with Hoechst 33258 ( $\lambda_{\text{em}}$  = 461 nm). Center column: PZn<sub>3</sub> anti-HER2-NIREPs ( $\lambda_{\text{em}}$  = 809 nm) located on the membrane surface and in the cell cytoplasm. Right column: Overlay of the micrographs from the blue and red channels.

In a separate DOD project (PI: Armstrong) it was found that NIREPs bearing antibodies targeted to EPCAM saw batch-to-batch variability in flow cytometry experiments for binding to EPCAM over-expressing cells. Investigation of new batches of anti-HER2-NIREPs found similar difficulties in reproducibility (Figure 2). In some batches, high uptake of up to 85,000 NIREPs per HER2+ SKBR3 cell were observed; in others, uptake levels matched that of control NIREPs conjugated to an isotype-matched IgG antibody. This prompted us to reinvestigate our protocols in detail. Our previously used bicinchoninic assay (BCA) used to determine the degree of antibody functionalization on the surface on the NIREP was unable to distinguish between covalently bound-antibody and surface associated antibody. Therefore, the use of this assay to determine the efficiency of different antibody-coupling chemistries in some cases may have yielded inaccurate data.

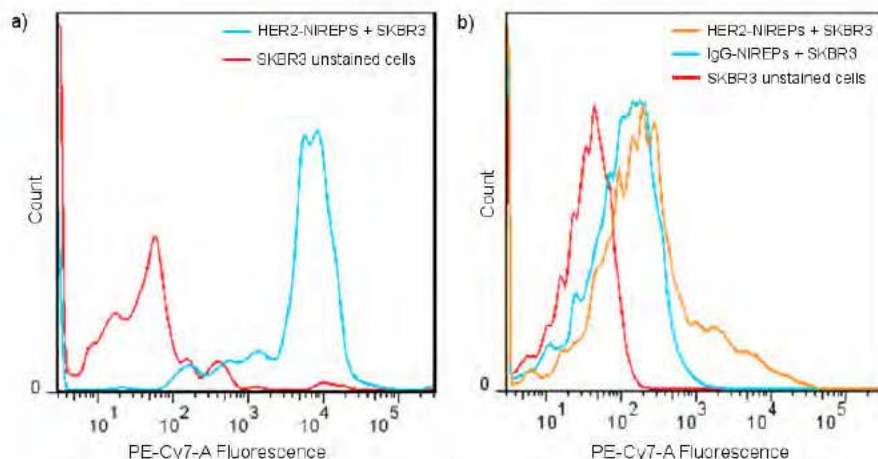
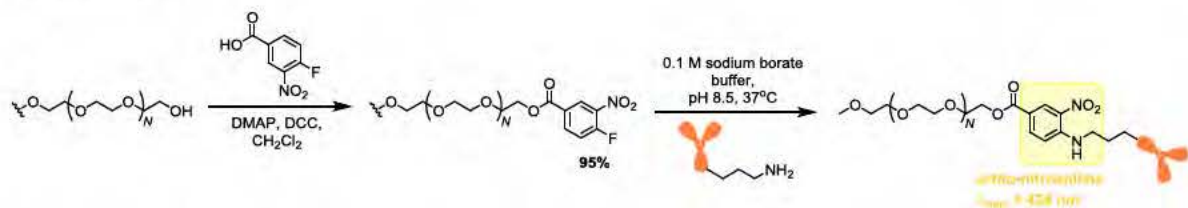


**Figure 2.** Flow sorting of HER2+ SKBR3 cells using anti-HER2-NIREPs; detection using the Cy7 channel (>790 nm near infrared wavelength). **a)** Batch 1: Large uptake of anti-HER2-NIREPs into SKBR3 cells gives a large increase in fluorescence compared to unstained cells; **b)** Batch 2: Negligible uptake of anti-HER2-NIREPs into SKBR3 cells, with very similar levels of fluorescence to cells incubated with control IgG-conjugated NIREPs.

We have therefore invested time optimizing our coupling protocols and characterization methods as described below.

### Antibody Conjugation Strategies

We have developed fluoronitrobenzoic acid (FNB)- based chemistry for the chemical conjugation of bioligands to the surface of NIREPs. The FNB group can be introduced onto the hydroxyl-terminus of a polymer in a single, high yielding step,<sup>19</sup> and unlike maleimide chemistries, is stable to hydrolysis at mild pHs (Scheme 1).



**Scheme 1.** Functionalization of PDB-*b*-PEO diblock copolymer OB18 with FNB. Conjugation of a bioligand via a lysine residue yields a chromophoric *ortho*-nitroaniline linker highlighted in yellow.

FNB is reactive to primary amines, which in the case of protein-based ligands, is readily available via the N-terminus or surface lysine residues. The abundance of these residues in proteins such as antibodies

(Abs) means prior chemical modification of Abs is unnecessary. The Therien group has previously used FNB-based chemistry to successfully functionalize NIREPs with the cell-penetrating Tat peptide for tracking dendritic cells (DCs) *in vivo*.<sup>20</sup> In this work, conjugation of Tat to the FNB-functionalized polymer was carried out *prior* to polymersome formation, allowing the conjugation to be carried out in organic solvents; progress of the reaction could be monitored by UV-vis absorption as the resulting *ortho*-nitroaniline chromophore absorbs at 428 nm (Scheme 1).<sup>19</sup> Presence of the peptide did not adversely affect the resulting polymersome morphology.

We have adapted this FNB-based chemistry for the conjugation of whole antibodies to the surface of polymersomes with these considerations: Conjugation to FNB must 1) be carried out under mild, aqueous conditions in order to preserve antibody functionality; 2) occur post-polymersome formation, as the large, hydrophilic nature of antibodies would likely disrupt the polymer's ability to form stable vesicle structures due to a vastly altered hydrophobic fraction.<sup>21</sup> It has already been demonstrated that polymersomes, once formed, are stable to surface decoration with Abs.<sup>22–24</sup>

Covalent modification of one of the many surface lysine residues present in Abs has the potential to affect antigen-recognition properties, either directly (through modification of residues in the complementarity determining region (CDR)) or indirectly through allosteric effects. Trastuzumab contains between 80–95 lysine residues which potentially can act as a chemical handle for direct attachment to FNB-NIREPs. Thus, the conjugation of trastuzumab with FNB-terminated tri(ethylene glycol) monomethyl ether (FNB-TEG) as a PEO- diblock copolymer model was explored. Trastuzumab was incubated with FNB-TEG at various molar ratios (40:1, 20:1, and 10:1 FNB-TEG to antibody) in sodium borate buffer, and the resulting Ab-TEG conjugates were analyzed using a statistical MALDI-MS method as reported previously (Figure 3).

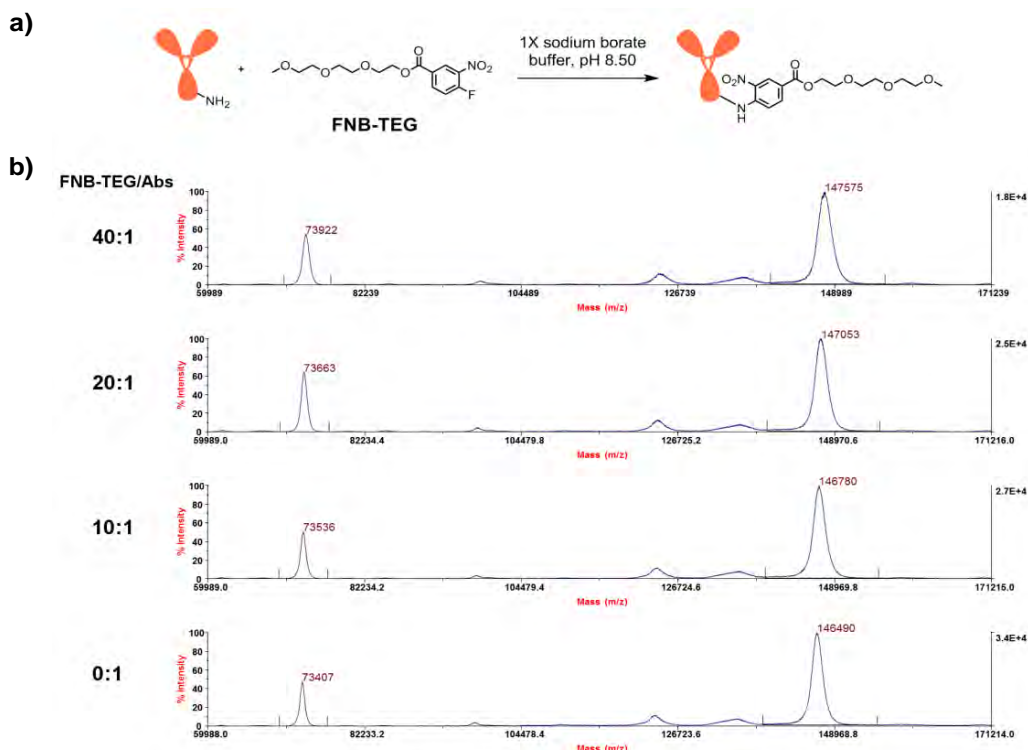


**Figure 3.** (a) Synthetic scheme for the modification of trastuzumab with FNB-TEG. (b) MALDI-MS of the resulting Ab-TEG conjugates where trastuzumab was incubated with FNB-TEG in a (from top to bottom) 1:40, 1:20, 1:10 and 1:0 (blank) ratio. Spectra were acquired in linear detection mode with a sinapinic acid matrix; peaks were calibrated to BSA.

Briefly, by acquiring a mass spectrum of each Ab-TEG preparation in replicates greater than 3, it is possible to detect a minimal mass difference of 119 Da between IgG and its corresponding conjugates to a 95% confidence level, even in linear detection mode.<sup>25</sup> The average number of moles of the conjugate attached per mole of IgG can be subsequently calculated from the difference in the observed masses of Ab-TEG conjugates and the unconjugated trastuzumab blank (0:1 preparation), divided by the molecular weight of the FNB-TEG conjugate. The results, summarized in Table 1, showed that we are able to reproducibly vary the degree of trastuzumab modification from 1 FNB-TEG group (10:1 preparation) to ~4–5 FNB-TEG groups (40:1 preparation).

FNB-TEG/Ab ratio	Mean mass by MALDI /Da <sup>†</sup>	Standard deviation /Da	Mass difference to native Ab /Da	Number of FNB-TEG conjugates	<i>p</i> value
40:1	148155	100	1394	4.5	<0.01
20:1	147479	140	719	2.3	<0.01
10:1	147129	147	368	1.2	0.02
0:1 <sup>‡</sup>	146761	139	0	0	–

**Table 1.** MALDI-MS results from the coupling of FNB-TEG model with trastuzumab. The degree of trastuzumab covalent modification could be reproducibly varied between ~1–4 TEG groups per Ab by varying the concentration of the FNB-functionalized reagent. <sup>†</sup> Data an average of three analyses. <sup>‡</sup> Blank sample. Trastuzumab was treated with sodium borate buffer under identical reaction conditions.

**Spector Group (June 2014–June 2015):** The antigen-recognition properties of the trastuzumab conjugates were assessed in an immunofluorescent assay using a human breast cancer cell line MCF10A following induction of HER2 expression using a doxycycline regulated promoter. The lentiviral doxycycline-inducible system was originally used to express short-hairpin RNA for gene expression suppression<sup>26</sup> but has been modified by the Spector group for

regulated expression of cloned cDNAs. The results showed that showed covalently modified trastuzumab retained antigen recognition properties (Figure 4). The antigen-binding activity was further quantified by MCF10A HER2+ extract nitrocellulose slot blot using a fluorescently labeled secondary anti-human IgG (Figure 5); trastuzumab coupled to an average of 2 TEG groups retained ~65% of its antigen reactivity, which was comparable to the blank sample incubated with conjugation buffer under the reaction conditions (~70%). These results showed that the reduction in antigen binding affinity is associated with handling the antibody (*e.g.* temperature, buffer, purification steps) rather than through modification of the CDR region. The conclusions from these experiments show that we are able to control the number of modifications made

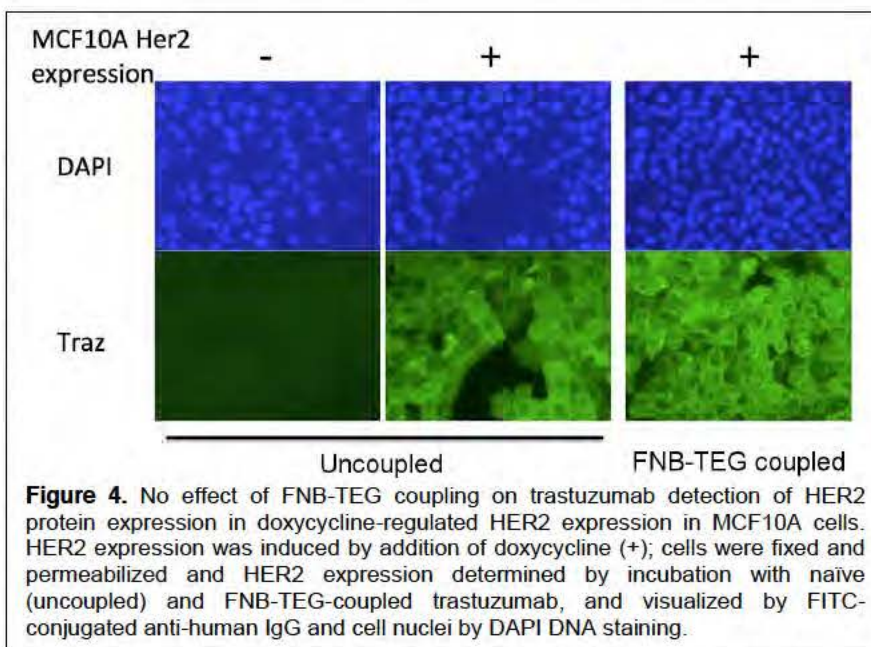
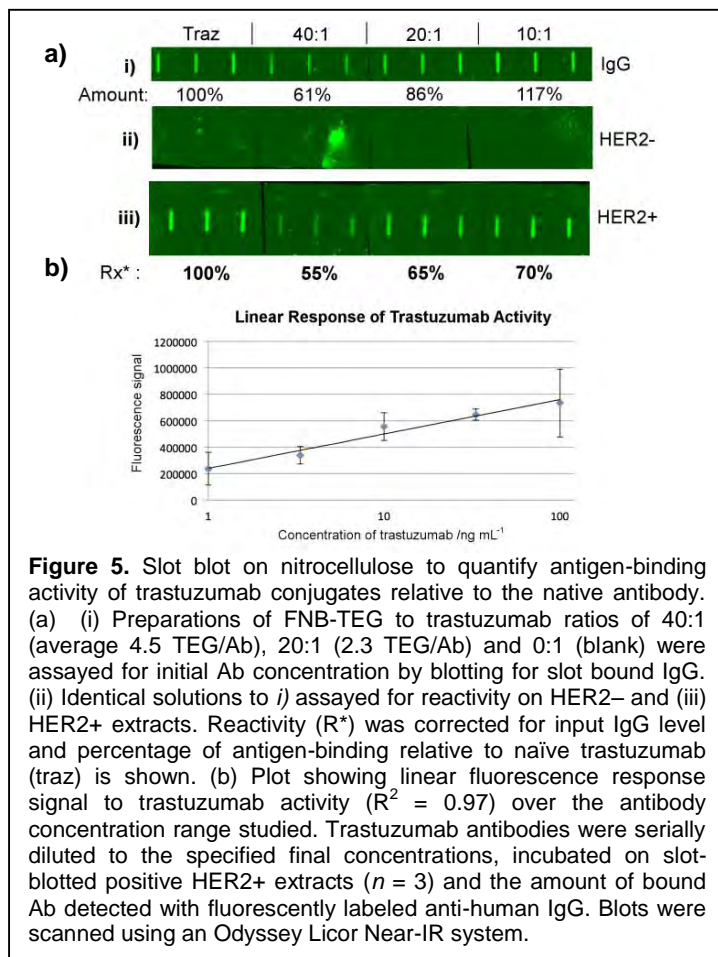
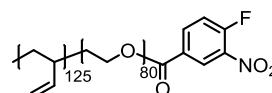


**Figure 4.** No effect of FNB-TEG coupling on trastuzumab detection of HER2 protein expression in doxycycline-regulated HER2 expression in MCF10A cells. HER2 expression was induced by addition of doxycycline (+); cells were fixed and permeabilized and HER2 expression determined by incubation with naive (uncoupled) and FNB-TEG-coupled trastuzumab, and visualized by FITC-conjugated anti-human IgG and cell nuclei by DAPI DNA staining.

on the surface of trastuzumab, and covalent attachment of a TEG chain does not occur in the antigen binding region. It is our expectation that we will be able to couple many copies of trastuzumab onto the surface of polymersomes. This, coupled with the demonstrated ability of surface-conjugated bioligands such as antibodies to cluster on fluid membrane polymersomes to maximise antigen binding affinity(ref) means that the multi-ligand effect of Ab-conjugated polymersomes should more than compensate for a ~30% drop in antigen binding affinity.

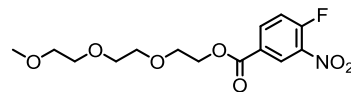


#### Synthesis of FNB-functionalized OB18 (PEO(3.9k)-b-PBD(6.5k))



OB18 (100.0 mg, 9.6  $\mu$ mol) was dissolved in toluene and dried by azeotropic distillation using a Dean Stark trap to remove residual water. In a separate dried flask, 4-fluoro-3-nitrobenzoic acid (7.1 mg, 38.4  $\mu$ mol),  $N,N'$ -dicyclohexylcarbodiimide (8.4 mg, 40.4  $\mu$ mol) and dimethylaminopyridine (0.1 mg, 0.7  $\mu$ mol) were dissolved in dry dichloromethane, stirred at rt for 30 min then cannulated into the OB18 distillate. After stirring for 2 d at rt, the solvent was removed under reduced pressure, and the resulting residue dissolved in THF and purified by size exclusion column to obtain the title compound.

#### Synthesis of FNB-TEG XX



Triethylene glycol monomethyl ether XX (292  $\mu$ L, 1.8 mmol), 4-fluoro-3-nitrobenzoic acid (405 mg, 2.2 mmol),  $N,N'$ -dicyclohexylcarbodiimide (490 mg, 2.4 mmol) and dimethylaminopyridine (27 mg, 0.21 mmol) were dissolved in dry dichloromethane (12.0 mL) and stirred at rt for 4 h until shown to be complete by TLC (5:100 MeOH/ $\text{CHCl}_3$ , Me-TEG  $R_f$  0.35; product  $R_f$  0.85; visualized by  $\text{KMnO}_4$  stain). The reaction mixture was filtered, and the resulting filtrate was washed consecutively with DI water, 5% AcOH in water, and water. The organic layer was dried with  $\text{MgSO}_4$ , concentrated then columned (silica, 9:1  $\text{CHCl}_3/\text{Et}_2\text{O}$ ,  $R_f$  0.29) to obtain the product as a colorless solid (548 mg, 91%);  $\delta_{\text{H}}$  (400 MHz,  $\text{CDCl}_3$ ), 8.73 (dd, 1H,  $J_1 = 7.2$ ,  $J_2 = 2.2$  Hz, Ar-H), 8.33 (ddd, 1H,  $J_1 = 8.7$ ,  $J_2 = 4.2$ ,  $J_3 = 2.2$ , Ar-H), 7.37 (dd, 1H,  $J_1 = 10.2$ ,  $J_2 = 8.7$ , Ar-H), 4.55–4.47 (m, 2H,  $\text{CH}_2$ ), 3.87–3.80 (m, 2H,  $\text{CH}_2$ ), 3.74–3.60 (m, 8H,  $\text{CH}_2$ ), 3.56–3.49 (m, 2H,  $\text{CH}_2$ ), 3.35 (s, 3H,  $\text{OCH}_3$ );  $\delta_{\text{H}}$  (400 MHz,  $\text{CDCl}_3$ ) –110.58 (ddd, 1F,  $J_1 = 10.4$ ,  $J_2 = 7.2$ ,  $J_3 = 4.3$ );  $m/z$  (ESI MS+) 332.1 ( $[\text{M}+\text{H}]^+$ ,  $\text{C}_{14}\text{H}_{19}\text{FNO}_7^+$ , requires 331.1).

#### Modification of antibodies with FNB-TEG

Trastuzumab (Genentech) was desalted into 1X sodium borate buffer (285 mOsm, pH 8.50) using a Amicon Ultra 0.5 mL 100 kDa MWCO Centrifugal Filter using the manufacturer's instructions. The desalted antibody was diluted to a 4 mg/mL concentration with buffer, and the concentration checked by UV-vis absorption at 280 nm (*vide supra*). FNB-TEG, dissolved in buffer, was added to the desalted antibody at molar ratios of 40:1, 20:1, or 10:1. The reactions were shaken at 750 rpm at 37 °C for 20 h, and then desalted into 1X PBS (285 mOsm, pH 7.40) for immunofluorescence studies, or MilliQ water for MALDI analysis.

NMR:

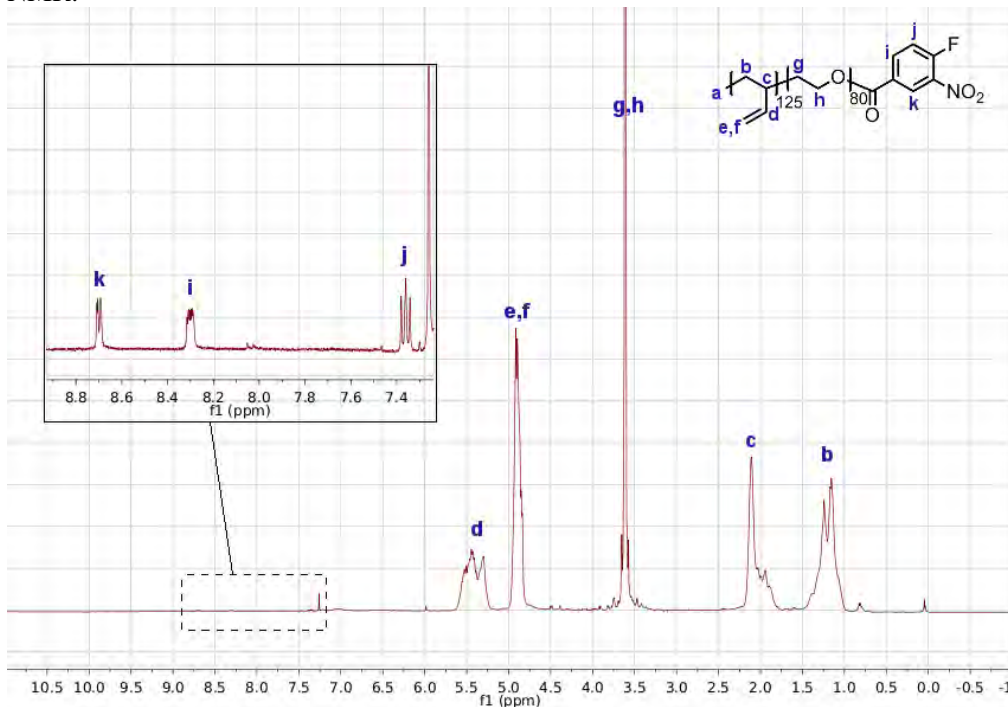


**Figure 6.**  $^1\text{H}$  NMR (500 MHz,  $\text{CDCl}_3$ , 298 K) of FNB-functionalized OB18.

#### *MALDI-MS analysis of trastuzumab-TEG conjugates*

MALDI-MS spectra were recorded on an AB Sciex 4800 Plus MALDI-ToF instrument in linear detection mode using a sinapinic acid matrix. For each sample, 3 separate mass spectra were obtained, and the peak maxima were averaged, and subtracted from that obtained from unmodified trastuzumab. The mass differences were divided by the molecular weight of the FNB-TEG conjugate to obtain the average degree of substitution per antibody.

#### *Immunofluorescence*

Cells were plated in complete media on 15 mm round uncoated glass coverslips. Cells were fixed in 3.7% formaldehyde/1X phosphate buffered saline (PBS), and permeabilized by incubation with a solution of 1% NP-40 detergent/PBS. For staining of cellular expressed HER2, cells were incubated with 400 ng/mL rabbit anti-HER2 antibody (Santa Cruz SC-284) / 100  $\mu\text{g/mL}$  bovine serum albumin/ 0.02% azide/PBS. Protein was visualized with AlexaFluor 488 goat anti-rabbit secondary antibody and imaged on Leica fluorescence.

### Slot blot

**Spector Group:** A protein solution of either HER2+/- cellular extracts or trastuzumab antibody was diluted in PBS and 200-400  $\mu$ L was added to a slot blot manifold applied under vacuum onto pre-wetted Protran nitrocellulose membranes. Membranes were dried and then incubated with a 5% non-fat dry milk (5% Blotto) in PBS for 1 h at room temperature to block unoccupied binding sites then incubated with either anti-human IgG-800 near-IR antibody (Molecular Probes/Life Technologies) or trastuzumab followed by anti-human IgG-800 in 1% Blotto. Following incubation with antibody solutions, non-specifically bound antibodies were removed by  $3 \times 15$  minute washes with PBS containing 0.05% Tween 20. The level of secondary antibody was determined by scanning on a LI-COR Odyssey near-IR blot scanner.

### NIREP construction

Using our newly validated functionalized OB18 polymer, we can construct NIREPs using our well-established methodology (Figure 7).

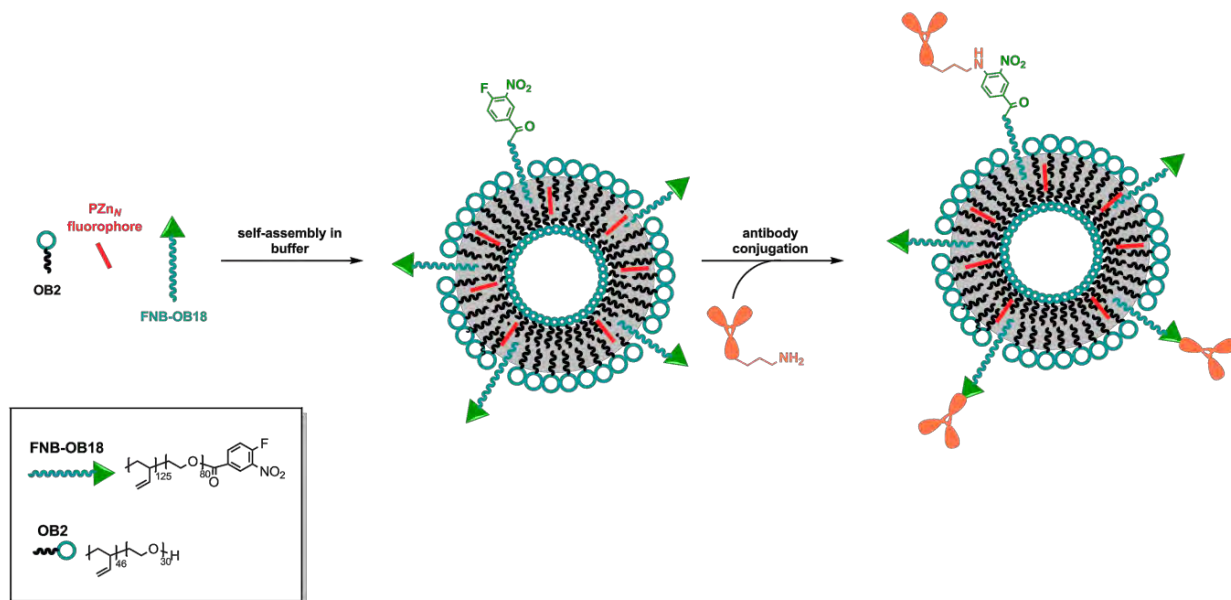
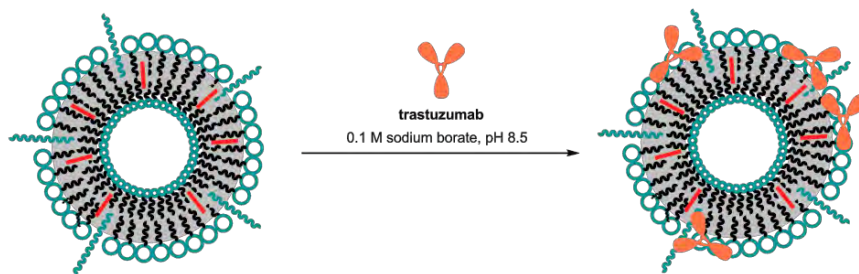


**Figure 7.** Construction of antibody-conjugated NIREPs.

NIREP synthesis was carried out using the thin-film hydration method as previously described.<sup>27-36</sup> An organic solution of FNB-functionalized PEO(3600)-b-PBD(6800) diblock copolymer (**FNB-OB18**), short-chain PEO(1300)-b-PBD(2500) (**OB2**) and PZn<sub>N</sub> NIRF at a 5:95:5 molar ratio was spotted onto a roughened Teflon plate and allowed to evaporate to form a uniformly coated surface. After residual solvent removal under high vacuum for >24h, 1X PBS buffer (285 mOsm, pH 7.40) is added and the films incubated at 60 °C for 24 h, followed by 90 minutes of sonication in a bath sonicator. Nanoscale, unilamellar NIREPs are subsequently obtained using procedures analogous to those used to formulate liposomes (sonication, freeze-thaw and extrusion). Ten freeze-thaw cycles are carried out by alternatively placing the samples in liquid N<sub>2</sub>, followed by a 5 minute sonication in a water bath at 60 °C. Extrusion through 400 nm polycarbonate membranes is carried out at 60°C using a thermobarrel extruder under moderate pressures. NIREP vesicle size and morphology is characterized by cryogenic transmission electron microscopy (cryo-TEM) and dynamic light scattering (DLS).

### Assessment of non-specific absorption

### Non-specific absorption:



### Covalent coupling plus non-specific absorption:

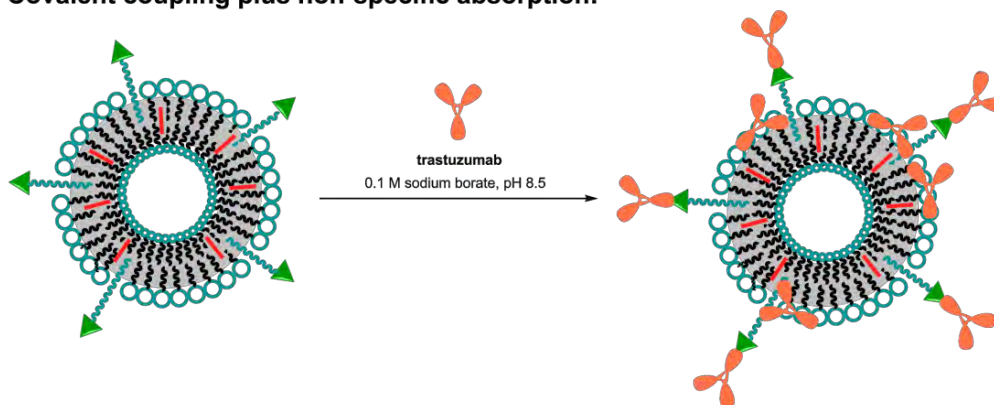


**Figure 8.** Assessing the degree of antibody non-specific absorption to the polymersomal surface.

Having validated that the variation in batches of Ab-NIREPs is not due to inadvertent deactivation of trastuzumab through covalent modification or conjugation conditions, we sought to quantify the degree of non-specific absorption of trastuzumab to the polymersome surface (Figure 8). To assess this, we incubated trastuzumab with unfunctionalized 5:95 OB18/OB2 polymersomes, under identical coupling and purification conditions to which we will carry out the Ab conjugation to FNB-functionalized NIREPs. Previously, we used the enhanced BCA assay to determine the protein content of our polymersome samples, which has a sensitivity range of 5–250  $\mu\text{g/mL}$  protein. However, on re-exploring our protocols, we have determined that at a polymersome concentration of 5  $\text{mg/mL}$ , the lower detection limit of 5  $\mu\text{g/mL}$  protein corresponds to approximately 19 antibodies/polymersome; we thus conclude that this assay is too insensitive for our needs. Unfortunately, we found that the micro-BCA assay, with an ideal detection range of 0.5–200  $\mu\text{g/mL}$  protein (corresponding to a lower detection range of 2 Abs/NIREP), is incompatible



**Figure 9.** Micro-BCA assay. Rows 1–3: dilution series of bovine gamma globulin (BGG) standards for protein content calibration. Rows 4–6: Samples A–C: polymersomes incubated with trastuzumab; Samples D–F: polymersomes only. Identical color for Samples A through F shows false positives for polymersome only samples.

with polymersomes resulting in false positives (Figure 9). The **Spector Group** developed a sensitive methodology for the detection of antibody concentration by Western blot analysis; Figure 10 shows a proof-of-principle experiment analyzing unfunctionalized NIREPs incubated with (Samples A–B; 1:1 molar ratio trastuzumab/OB18) and without (Samples C–D) trastuzumab. The fluorescently labeled anti-human secondary IgG antibody shows linear sensitivity over a wide range of trastuzumab concentrations and is capable of detecting as little as 0.1 ng Ab.

#### *Coupling strategy to assess degree of non-specific absorption*

Unfunctionalized 5:95 OB18/OB2 NIREPs were desalted into 1X sodium borate buffer (pH 8.50, 285 mOsm), and concentrated to ~5 mg/mL concentration by centrifugal filtration (Amicon Ultra 4 mL 100 kDa MWCO centrifugal filter). The polymersome concentration was determined by UV-vis absorption of the sample corrected for scattering, using previously determined extinction coefficients.<sup>32</sup> Similarly, trastuzumab (Genentech) was desalted into 1X sodium borate, and concentrated to a ~10 mg/mL concentration by centrifugal filtration; concentration was determined by absorption at 280 nm. Desalted trastuzumab and NIREP were combined at fixed molar ratios (e.g. 40:1 molar ratio of OB18 to trastuzumab) and agitated at 750 rpm for 24 h at 37 °C. The reaction mixture was purified on a Sephacryl S-500 column with 1X PBS (1 mL/min, detection at 280, 426 and 700 nm). Purified NIREP fractions were combined and concentrated to ~5 mg/mL concentration by centrifugal filtration.

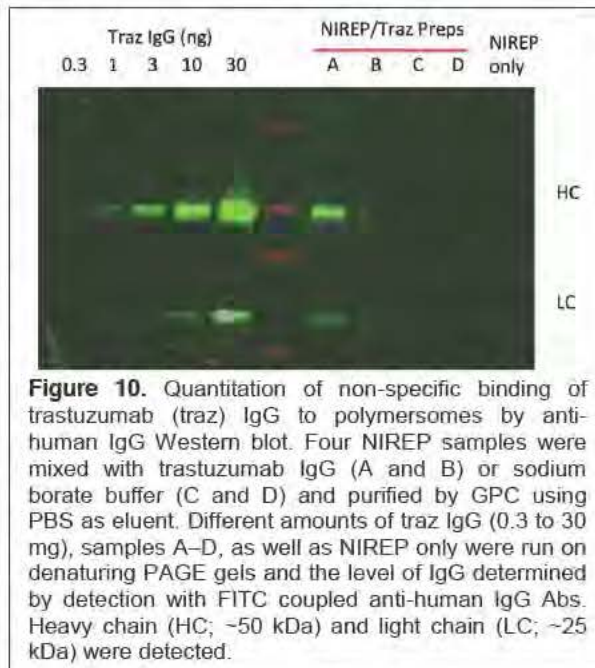


**Figure 10.** Quantitation of non-specific binding of trastuzumab (traz) IgG to polymersomes by anti-human IgG Western blot. Four NIREP samples were mixed with trastuzumab IgG (A and B) or sodium borate buffer (C and D) and purified by GPC using PBS as eluent. Different amounts of traz IgG (0.3 to 30 mg), samples A–D, as well as NIREP only were run on denaturing PAGE gels and the level of IgG determined by detection with FITC coupled anti-human IgG Abs. Heavy chain (HC; ~50 kDa) and light chain (LC; ~25 kDa) were detected.

#### *Assessing protein content of NIREPs*

The amount of trastuzumab bound/coupled to a NIREP was determined by Western blotting. Samples, and a dilution series of known quantities of pure trastuzumab antibody were denatured with laemlli denaturing buffer, sized on denature PAGE gel, and transferred to nitrocellulose using an iBlott transfer apparatus (LifeTechnology). The membrane was blocked with 5% Blotto for 1 h at room temperature then incubated with anti-human IgG-800 antibody in 1% Blotto. Non-specifically bound antibodies were removed by 3 × 15 minute washes with PBS containing 0.05% Tween 20 and the level of trastuzumab signal was determined by scanning on a LI-COR Odyssey near-IR blot scanner. A calibration plot of the diluted trastuzumab was determined and the amount of trastuzumab in each NIREP preparation was calculated.

Final NIREP concentration, determined by UV-vis as described above, was converted into average number of particles per unit volume,  $N$ , using the following equation:<sup>37</sup>

$$N = \frac{6 \times W \times 10^{-3}}{\pi \times (D_o^3 - D_i^3) \times 10^{-21} \times \rho} \quad (1)$$

Where  $W$  is the polymer mass (in mg/mL),  $D_o$  is the average outer diameter of the polymersome (obtained by DLS),  $D_i$  is the diameter of the polymersome lumen (calculated  $D_o - 2l$ , where  $l$  is the polymersome membrane thickness, determined by cryo-TEM),<sup>38</sup> and  $\rho$  is the density of OB2 (previously determined as

1.08 g/cm<sup>3</sup>).<sup>39</sup> The concentration of trastuzumab in the sample,  $Y$ , determined by Western blot analysis, is converted to number of antibodies,  $M$ :

$$M = \frac{Y \times 10^{-6}}{mw} \times N_A \quad (2)$$

Where  $mw$  is the molecular weight of trastuzumab (145,531 g/mol) and  $N_A$  is Avogadro's constant. The number of antibodies per polymersome is thus calculated  $M/N$ . Samples were measured in triplicate.

## Bibliography.

- (1) Perou, C. M.; Sørli, T.; Eisen, M. B.; Rijn, M. van de; Jeffrey, S. S.; Rees, C. A.; Pollack, J. R.; Ross, D. T.; Johnsen, H.; Akslen, L. A.; Fluge, Ø.; Pergamenschikov, A.; Williams, C.; Zhu, S. X.; Lønning, P. E.; Børresen-Dale, A.-L.; Brown, P. O.; Botstein, D. *Nature* **2000**, *406* (6797), 747.
- (2) Sørli, T.; Perou, C. M.; Tibshirani, R.; Aas, T.; Geisler, S.; Johnsen, H.; Hastie, T.; Eisen, M. B.; Rijn, M. van de; Jeffrey, S. S.; Thorsen, T.; Quist, H.; Matese, J. C.; Brown, P. O.; Botstein, D.; Lønning, P. E.; Børresen-Dale, A.-L. *Proc. Natl. Acad. Sci.* **2001**, *98* (19), 10869.
- (3) Slamon, D. J.; Clark, G. M.; Wong, S. G.; Levin, W. J.; Ullrich, A.; McGuire, W. L. *Science* **1987**, *235* (4785), 177.
- (4) Slamon, D. J.; Leyland-Jones, B.; Shak, S.; Fuchs, H.; Paton, V.; Bajamonde, A.; Fleming, T.; Eiermann, W.; Wolter, J.; Pegram, M.; Baselga, J.; Norton, L. *N. Engl. J. Med.* **2001**, *344* (11), 783.
- (5) Hynes, N. E.; Lane, H. A. *Nat. Rev. Cancer* **2005**, *5* (5), 341.
- (6) Early Breast Cancer Trialists' Collaborative Group (EBCTCG). *The Lancet* **2011**, *378* (9793), 771.
- (7) Nabholz, J.-M.; Mouret-Reynier, M.-A.; Durando, X.; Van Praagh, I.; Al-Sukhun, S.; Ferriere, J.-P.; Chollet, P. *Expert Opin. Pharmacother.* **2009**, *10* (9), 1435.
- (8) Dowsett, M.; Cuzick, J.; Ingle, J.; Coates, A.; Forbes, J.; Bliss, J.; Buyse, M.; Baum, M.; Buzdar, A.; Colleoni, M.; Coombes, C.; Snowdon, C.; Gnant, M.; Jakesz, R.; Kaufmann, M.; Boccardo, F.; Godwin, J.; Davies, C.; Peto, R. *J. Clin. Oncol.* **2010**, *28* (3), 509.
- (9) Lower, E. E.; Glass, E.; Blau, R.; Harman, S. *Breast Cancer Res Treat* **2009**, *113* (2), 301.
- (10) Valabrega, G.; Montemurro, F.; Aglietta, M. *Ann. Oncol.* **2007**, *18* (6), 977.
- (11) Osborne, C. K.; Schiff, R. *Annu. Rev. Med.* **2011**, *62* (1), 233.
- (12) Xia, W.; Bacus, S.; Hegde, P.; Husain, I.; Strum, J.; Liu, L.; Paulazzo, G.; Lyass, L.; Trusk, P.; Hill, J.; Harris, J.; Spector, N. L. *Proc. Natl. Acad. Sci.* **2006**, *103* (20), 7795.
- (13) Xia, W.; Liu, Z.; Zong, R.; Liu, L.; Zhao, S.; Bacus, S. S.; Mao, Y.; He, J.; Wulfschle, J. D.; Petricoin, E. F.; Osada, T.; Yang, X.-Y.; Hartman, Z. C.; Clay, T. M.; Blackwell, K. L.; Lyster, H. K.; Spector, N. L. *Mol. Cancer Ther.* **2011**, *10* (8), 1367.
- (14) Eichhorn, P. J. A.; Gili, M.; Scaltriti, M.; Serra, V.; Guzman, M.; Nijkamp, W.; Beijersbergen, R. L.; Valero, V.; Seoane, J.; Bernards, R.; Baselga, J. *Cancer Res.* **2008**, *68* (22), 9221.
- (15) Rexer, B. N.; Ham, A.-J. L.; Rinehart, C.; Hill, S.; de Matos Granja-Ingram, N.; González-Angulo, A. M.; Mills, G. B.; Dave, B.; Chang, J. C.; Liebler, D. C.; Arteaga, C. L. *Oncogene* **2011**, *30* (40), 4163.
- (16) Garrett, J. T.; Olivares, M. G.; Rinehart, C.; Granja-Ingram, N. D.; Sanchez, V.; Chakrabarty, A.; Dave, B.; Cook, R. S.; Pao, W.; McKinley, E.; Manning, H. C.; Chang, J.; Arteaga, C. L. *Proc. Natl. Acad. Sci.* **2011**, *108* (12), 5021.
- (17) Kurokawa, M.; Kim, J.; Geradts, J.; Matsuura, K.; Liu, L.; Ran, X.; Xia, W.; Ribar, T. J.; Henao, R.; Dewhirst, M. W.; Kim, W.-J.; Lucas, J. E.; Wang, S.; Spector, N. L.; Kornbluth, S. *Sci. Signal.* **2013**, *6* (274), ra32.
- (18) Xia, W.; Petricoin, E. F.; Zhao, S.; Liu, L.; Osada, T.; Cheng, Q.; Wulfschle, J. D.; Gwin, W. R.; Yang, X.; Gallagher, R. I.; Bacus, S.; Lyster, H.; Spector, N. L. *Breast Cancer Res.* **2013**, *15* (5), R85.
- (19) Ladd, D. L.; Snow, R. A. *Anal. Biochem.* **1993**, *210* (2), 258.

- (20) Christian, N. A.; Benencia, F.; Milone, M. C.; Li, G.; Frail, P. R.; Therien, M. J.; Coukos, G.; Hammer, D. A. *Mol. Imaging Biol.* **2009**, *11* (3), 167.
- (21) Levine, D. H.; Ghoroghchian, P. P.; Freudenberg, J.; Zhang, G.; Therien, M. J.; Greene, M. I.; Hammer, D. A.; Murali, R. *Methods* **2008**, *46* (1), 25.
- (22) Lin, J. J.; Ghoroghchian, P. P.; Zhang, Y.; Hammer, D. A. *Langmuir* **2006**, *22* (9), 3975.
- (23) Robbins, G. P.; Saunders, R. L.; Haun, J. B.; Rawson, J.; Therien, M. J.; Hammer, D. A. *Langmuir* **2010**, *26* (17), 14089.
- (24) Hammer, D. A.; Robbins, G. P.; Haun, J. B.; Lin, J. J.; Qi, W.; Smith, L. A.; Ghoroghchian, P. P.; Therien, M. J.; Bates, F. S. *Faraday Discuss* **2008**, *139*, 129.
- (25) Ogawa, Y.; Traina, J.; Zimmermann, E.; Yu, T.; Schneider, D. W.; Pungor, E. *Anal. Biochem.* **2007**, *368* (2), 214.
- (26) Shin, K.-J.; Wall, E. A.; Zavzavadjian, J. R.; Santat, L. A.; Liu, J.; Hwang, J.-I.; Rebres, R.; Roach, T.; Seaman, W.; Simon, M. I.; Fraser, I. D. C. *Proc. Natl. Acad. Sci.* **2006**, *103* (37), 13759.
- (27) Ghoroghchian, P. P.; Li, G.; Levine, D. H.; Davis, K. P.; Bates, F. S.; Hammer, D. A.; Therien, M. J. *Macromolecules* **2006**, *39* (5), 1673.
- (28) Ghoroghchian, P. P.; Frail, P. R.; Li, G.; Zupancich, J. A.; Bates, F. S.; Hammer, D. A.; Therien, M. J. *Chem. Mater.* **2007**, *19* (6), 1309.
- (29) Qi, W.; Ghoroghchian, P. P.; Li, G.; Hammer, D. A.; Therien, M. J. *Nanoscale* **2013**, *5* (22), 10908.
- (30) Katz, J. S.; Eisenbrown, K. A.; Johnston, E. D.; Kamat, N. P.; Rawson, J.; Therien, M. J.; Burdick, J. A.; Hammer, D. A. *Soft Matter* **2012**, *8* (42), 10853.
- (31) Ghoroghchian, P. P.; Frail, P. R.; Susumu, K.; Blessington, D.; Brannan, A. K.; Bates, F. S.; Chance, B.; Hammer, D. A.; Therien, M. J. *Proc. Natl. Acad. Sci.* **2005**, *102* (8), 2922.
- (32) Ghoroghchian, P. P.; Frail, P. R.; Susumu, K.; Park, T.-H.; Wu, S. P.; Uyeda, H. T.; Hammer, D. A.; Therien, M. J. *J. Am. Chem. Soc.* **2005**, *127* (44), 15388.
- (33) Christian, N. A.; Milone, M. C.; Ranka, S. S.; Li, G.; Frail, P. R.; Davis, K. P.; Bates, F. S.; Therien, M. J.; Ghoroghchian, P. P.; June, C. H.; Hammer, D. A. *Bioconjug. Chem.* **2007**, *18* (1), 31.
- (34) Ghoroghchian, P. P.; Lin, J. J.; Brannan, A. K.; Frail, P. R.; Bates, F. S.; Therien, M. J.; Hammer, D. A. *Soft Matter* **2006**, *2* (11), 973.
- (35) Duncan, T. V.; Ghoroghchian, P. P.; Rubtsov, I. V.; Hammer, D. A.; Therien, M. J. *J Am Chem Soc* **2008**, *130* (30), 9773.
- (36) Sood, N.; Jenkins, W. T.; Yang, X.-Y.; Shah, N. N.; Katz, J. S.; Koch, C. J.; Frail, P. R.; Therien, M. J.; Hammer, D. A.; Evans, S. M. *J. Pharm.* **2013**, *2013*, 1.
- (37) Pang, Z.; Lu, W.; Gao, H.; Hu, K.; Chen, J.; Zhang, C.; Gao, X.; Jiang, X.; Zhu, C. *J. Controlled Release* **2008**, *128* (2), 120.
- (38) Bermudez, H.; Brannan, A. K.; Hammer, D. A.; Bates, F. S.; Discher, D. E. *Macromolecules* **2002**, *35* (21), 8203.
- (39) Ahmed, F.; Discher, D. E. *J. Controlled Release* **2004**, *96* (1), 37.

### 3.3 What opportunities for training and professional development has the project provided?

#### • Training

Melanie O'Sullivan (Postdoctoral Research Associate)

Training in colloidal synthesis and characterization including cryogenic transmission electron microscopy; biological techniques; imaging, in vitro biology.

#### • Professional development

Melanie O'Sullivan (Postdoctoral Research Associate)

Attendance at conferences and seminars listed under major activities. In addition, attended a grant writing workshop “Writing a Convincing Research Plan” at Duke University. Grant writing experience. Dr. O’Sullivan has had the opportunity to acquire very broad interdisciplinary training (e.g., nanoscale science, cancer biology, in vitro and in vivo imaging, cellular biology). She has learned new science and developed important new technologies, built networks of collaborators and contacts, learnt important skills for working in interdisciplinary environments, and is thus better equipped for a future career and leadership role in science, technology, and medicine.

### **3.4 How were the results disseminated to communities of interest?**

One manuscript detailing new fluorophores relevant to NIREP fabrication was published (Design of Diethynyl Porphyrin Derivatives with High NIR Fluorescence Quantum Yields, K. Susumu and M. J. Therien, *J. Porphyrins Phthalocyanines* **2015**, *19*, 205–218. DOI: 10.1142/S1088424614501107).

### **3.5 What do you plan to do during the next reporting period to accomplish the goals?**

Our next step is to apply the methodology described in Section 3.2 using FNB-functionalized NIREPs to generate anti-HER2-NIREPs. The degree of covalently coupled antibodies will be determined by subtracting the number of non-specifically absorbed antibodies, determined from the experiments previously described. With anti-HER2 NIREPs in hand, we will determine uptake into HER2– and HER2+ MCF10A cells (expression of HER2 regulated by dox, see Figure 4), by analyzing fluorescence intensity per cell by ImageStream flow cytometry.

We will then use our established roadmap for the fabrication of antibody-conjugated NIREPs to generate annexin-V NIREPs for the analysis of apoptosis in parental and lapatinib-resistant breast cancer cell lines when treated with lapatinib. Furthermore, we will profile the phenotypic changes associated with lapatinib resistance by fabricating CD146- and E-cadherin-targeted NIREPs.

## **4. IMPACT**

### **4.1 What was the impact on the development of the principal discipline(s) of the project?**

Breast cancer is not a single disease: it can be categorized into a series of subtypes dependent on which faulty protein or proteins in the cell are responsible for uncontrolled growth of the tumor. For example, tumors that overproduce the HER2 protein are called HER2+ tumors; this subtype of breast cancer is associated with a higher likelihood of the disease spreading, thus a lower life expectancy. Over the past 15 years, significant advancements in the treatment of breast cancer have been made by recognition that not all breast cancers are the same. Drugs such as trastuzumab or lapatinib have been designed to inhibit a specific faulty protein; this selectivity reduces the number of harmful side effects, while halting growth of the tumor. Despite these advances, in 2010, there were approximately 438,000 deaths worldwide due to breast cancer, the vast majority of these as a result of the cancer spreading. One major issue is that the primary tumor in the breast may differ in subtype to other tumors found elsewhere in the body. In addition, tumor cells that initially respond to treatment can evolve to become resistant to the effects of the drug, leading to disease recurrence, and this remains a significant problem in the treatment of breast cancer. The mechanisms by which the cells become resistant to these drugs are numerous and not fully understood; the situation is further complicated by the fact that tumors found elsewhere in the body may evolve in different ways in response to treatment. This complexity makes the design of new therapy regimens that circumvent drug resistance currently difficult. The inability to biopsy every tumor at regular time intervals in a patient with advanced breast cancer remains a significant impediment towards delivering an effective personalized

approach to the treatment of advanced stage breast cancer. *This research will develop the first non-invasive imaging method that allows tumors to be characterized into subtypes, without the need for a biopsy. Our system uses non-toxic, biodegradable nanoparticles (called “NIREPs”), which when injected, selectively recognize proteins on the surface of cells that mark the cell as cancerous, and transmit information about the cell using non-harmful frequencies of light that can be detected from outside of the body. We will develop NIREPs that can distinguish between different breast cancer subtypes, including which cancers are likely to respond to or be resistant to therapy. The non-invasive nature of this technology will allow us to study the evolution of therapy resistance over time: by understanding how tumors respond to therapy, more effective treatment regimens can be developed that will delay or halt the development of drug resistance, drastically improving patient survival and remission rates.* Importantly, we expect this platform to exhibit sufficient sensitivity to detect microscopic sites of metastatic disease that are currently undetectable by conventional patient imaging methods such as MRI or PET. Approximately 20–30% of women with early stage breast cancer have such tumors in their bone marrow; such patients have poorer prognosis for survival. Early detection of these sites and prompt intervention through an informed treatment program would drastically improve patient survival and remission rates.

We expect that once our methodology for the synthesis of antibody-conjugated NIREPs is established, it will provide a roadmap for future research in this area.

#### **4.2 What was the impact on other disciplines?**

Nothing to report.

#### **4.3 What was the impact on technology transfer?**

Nothing to report.

#### **4.4 What was the impact on society beyond science and technology?**

Dr. O’Sullivan, a young Ph.D. scientist, has been exposed to research challenges, experimental methods, research investigators, collaborators, and a research environment that will strongly influence her future career directions in the field of breast cancer research.

### **5. CHANGES/PROBLEMS**

#### **5.1 Changes in approach and reasons for change**

Nothing to report.

#### **5.2 Actual or anticipated problems or delays and actions or plans to resolve them**

Nothing to report.

#### **5.3 Changes that had a significant impact on expenditures**

Nothing to report.

#### **5.4 Significant changes in use or care of human subjects, vertebrate animals, biohazards, and/or select agents**

Nothing to report.

#### **5.5 Significant changes in use or care of human subjects**

Nothing to report.

#### **5.6 Significant changes in use or care of vertebrate animals.**

Nothing to report.

#### **5.7 Significant changes in use of biohazards and/or select agents**

Nothing to report.

### **6. PRODUCTS**

#### **6.1 Publications, conference papers, and presentations**

- **Journal publications.**

- 1) Design of Diethynyl Porphyrin Derivatives with High NIR Fluorescence Quantum Yields, K. Susumu and M. J. Therien, *J. Porphyrins Phthalocyanines*. **2015**, 19, 205–218. DOI: 10.1142/S1088424614501107; Published; Federal support acknowledged.

- **Other publications, conference papers, and presentations.**

- Presentations

- 1) “Antibody-Targeted Near-IR Emissive Polymersomes for the Non-Invasive Molecular Profiling of Tumors”, given at *Imaging in 2020 IX: Imaging and the Immune System, Jackson Hole, Wyoming*, September 21<sup>st</sup>, 2014.
- 2) “Nanoscale Agents for Optical Imaging”, given at the *Department of Chemistry, St. Michael’s College, Colchester, Vermont*, October 3<sup>rd</sup>, 2014.
- 3) “Tumor Delivery of Polymersome-Encapsulated Myoglobin Results in Rapid Intratumoral Hemorrhaging”, given at the *12th International Nanomedicine & Drug Delivery Symposium, University of North Carolina at Chapel Hill, Chapel Hill, North Carolina*, October 6<sup>th</sup>, 2014.
- 4) “Antibody-Targeted Near-IR Emissive Polymersomes for the Non-Invasive Molecular Profiling of Tumors”, given at the *Duke Cancer Institute 2nd Annual Scientific Retreat, Duke University, Durham, North Carolina*, November 14<sup>th</sup>, 2014.
- 5) “Tumor Delivery of Polymersome-Encapsulated Myoglobin Results in Rapid Intratumoral Hemorrhaging”, given at the *Duke Cancer Institute 2<sup>nd</sup> Annual Scientific Retreat, Duke University, Durham, North Carolina*, November 14<sup>th</sup>, 2014.
- 6) “Nanoscale Agents for Optical Imaging”, given at the *Department of Chemistry, University of Kentucky, Lexington, Kentucky*, January 23<sup>rd</sup>, 2015.

7) “Antibody-Targeted Near-IR Emissive Polymersomes for the Non-Invasive Molecular Profiling of Tumors”, given at *Cancer Nanotechnology: Nanomedicines from Laboratory to Clinical Reality*, West Dover, Vermont, June 29<sup>th</sup>, 2015.

## 6.2 Website(s) or other Internet site(s)

Nothing to report.

## 6.3 Technologies or techniques

Nothing to report.

## 6.4 Inventions, patent applications, and/or licenses

Nothing to report.

## 6.5 Other Products

Nothing to report.

# 7. PARTICIPANTS & OTHER COLLABORATING ORGANIZATIONS

## 7.1 What individuals have worked on the project?

Name:	<b>Michael J. Therien</b>
Project Role:	<i>PD/PI</i>
Researcher Identifier (e.g. ORCID ID):	<i>0000-0003-4876-0036</i>
Nearest person month worked:	<i>1 Summer Month</i>
Contribution to Project:	<i>Professor Therien is responsible for the overall administration and direction of the project. He plans experiments, interprets data, and writes papers and reports. Ongoing effort is devoted through research meetings, discussions, and collaborative research activities with Partnering PI Spector, and other project researchers</i>
Funding Support:	<i>Duke funds, NIH, DOE, DOD/Army, Homeland Security, USAMRAA, NSF, and Coulter Foundation</i>
Name:	<b>Melanie C. O’Sullivan</b>
Project Role:	<i>Research Associate</i>
Researcher Identifier (e.g. ORCID ID):	<i>0000-0001-8689-1059</i>
Nearest person month worked:	<i>1 Calendar Month</i>
Contribution to Project:	<i>Dr. O’Sullivan is responsible for all aspects of polymersome assembly, functionalization, and targeting.</i>

	<i>These responsibilities include, for example: diblock copolymer and fluorophore synthesis, purification of diblock copolymers functionalized with PEO-terminated reactive groups appropriate for antibody coupling reactions, assembly of polymersomes having diameters <math>\leq 100</math> nm that are derived from these materials, and the fabrication and characterization of nanoscale near infrared (NIR) emissive polymersomes (NIREPs) that have reactive and targeted surface functionality.</i>
Funding Support:	<i>Duke funds, DOD/Army and USARMAA</i>
Name:	<b><i>Joshua Stecher</i></b>
Project Role:	<i>Postdoctoral Associate</i>
Researcher Identifier (e.g. ORCID ID):	<i>0000-0001-9937-3509</i>
Nearest person month worked:	<i>2 Calendar months</i>
Contribution to Project:	<i>Dr. Stecher is responsible for synthesis of nanoscale agents for in vivo imaging, and the spectroscopic and physical characterization of these compositions.</i>
Funding Support:	<i>Duke funds, Homeland Security, USARMAA, and Coulter</i>

## 7.2 Has there been a change in the active other support of the PD/PI(s) or senior/key personnel since the last reporting period?

There are some changes for PI's active supports since last reporting period. Please see updated other support in the Appendices with changes highlighted.

## 7.3 What other organizations were involved as partners?

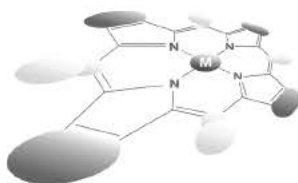
Nothing to report.

## 8. SPECIAL REPORTING REQUIREMENTS

COLLABORATIVE AWARDS: The Partnering PI, Dr. Neil Spector will submit his report.

## 9. APPENDICES

- Publication
- PI's biosketch
- PI's updated other support



## Design of diethynyl porphyrin derivatives with high near infrared fluorescence quantum yields

Kimihiro Susumu<sup>a,c,d</sup> and Michael J. Therien<sup>\*b,d</sup>

<sup>a</sup>Department of Chemistry, 231 South 34th Street, University of Pennsylvania, Philadelphia, PA 19104-6323, USA

<sup>b</sup>Department of Chemistry, French Family Science Center, 124 Science Drive, Duke University, Durham, NC 27708-0346, USA

*Dedicated to Professor Shunichi Fukuzumi on the occasion of his retirement*

Received 6 October 2014

Accepted 11 November 2014

**ABSTRACT:** A design strategy for (porphinato)zinc-based fluorophores that possess large near infrared fluorescence quantum yields is described. These fluorophores are based on a (5,15-diethynylporphinato) zinc(II) framework and feature symmetric donor or acceptor units appended at the *meso*-ethynyl positions via benzo[c][1,2,5]thiadiazole moieties. These (5,15-bis(benzo[c][1',2',5']thiadiazol-4'-ylethynyl)-10,20-bis[2',6'-bis(3'',3''-dimethyl-1''-butyloxy)phenyl]porphinato)zinc(II) (4), (5,15-bis[4'-(*N,N*-dihexylamino)benzo[c][1',2',5']thiadiazol-7'-ylethynyl]-10,20-bis[2',6'-bis(3'',3''-dimethyl-1''-butyloxy)phenyl]porphinato)zinc(II) (5), (5,15-bis([7'-(4''-*n*-dodecyloxyphenylethynyl)benzo[c][1',2',5']thiadiazol-4'-yl]ethynyl)-10,20-bis[2',6'-bis(3'',3''-dimethyl-1''-butyloxy)phenyl]porphinato)zinc(II) (6), (5,15-bis([7'-(4''-*n*-dodecyloxyphenyl)benzo[c][1'',2'',5'']thiadiazol-4''-yl]ethynyl)benzo[c][1',2',5']thiadiazol-4'-yl]ethynyl)-10,20-bis[2',6'-bis(3'',3''-dimethyl-1''-butyloxy)phenyl]porphinato)zinc(II) (7), 5,15-bis([7'-(4''-*N,N*-dihexylaminophenylethynyl)benzo[c][1',2',5']thiadiazol-4'-yl]ethynyl)-10,20-bis[2',6'-bis(3'',3''-dimethyl-1''-butyloxy)phenyl]porphinato)zinc(II) (8), and (5,15-bis([7'-(4''-*N,N*-dihexylaminophenylethynyl)benzo[c][1',2',5']thiadiazol-4'-yl]ethynyl)-10,20-bis[2',6'-bis(3'',3''-dimethyl-1''-butyloxy)phenyl]porphinato)zinc(II) (9) chromophores possess red-shifted absorption and emission bands that range between 650 and 750 nm that bear distinct similarities to those of the chlorophylls and structurally related molecules. Interestingly, the measured radiative decay rate constants for these emitters track with the integrated oscillator strengths of their respective x-polarized Q-band absorptions, and thus define an unusual family of high quantum yield near infrared fluorophores in which emission intensity is governed by a simple Strickler–Berg dependence.

**KEYWORDS:** diethynylporphyrin, benzo[c][1,2,5]thiadiazole, near infrared, fluorescence quantum yield, Strickler–Berg.

## INTRODUCTION

The design and synthesis of near infrared (NIR) absorption materials that possess large absorptive

oscillator strengths and high fluorescence quantum yields are important to molecular imaging [1–5] and solar energy conversion technologies [6–10]. Likewise, the efficient utilization of NIR sunlight is a key feature of natural photosynthesis, which exploits NIR-absorbing dyes such as chlorophylls and pheophytins [11]. Relative to the tremendous attention that has been paid to the design and synthesis of low band gap chromophores and materials [12–19], much less focus has been given to the development of strategies that channel enhanced oscillator strength into the low energy optical transitions

<sup>§</sup>SPP full member in good standing

\*Correspondence to: Michael J. Therien, tel: +1 919-660-1670, email: michael.therien@duke.edu

Current address: <sup>c</sup>Optical Sciences Division, U.S. Naval Research Laboratory, Washington, DC 20375, USA; <sup>d</sup>Sotera Defense Solutions, Inc., Columbia, MD 21046, USA

of such compositions. For example, only a limited number of conjugated organic structures possess both high oscillator strength NIR ( $S_0 \rightarrow S_1$ ) absorptions and corresponding high ( $S_1 \rightarrow S_0$ ) fluorescence quantum yields [20, 21]. In general, a higher  $S_0 \rightarrow S_1$  absorptive extinction coefficient should correlate with a larger  $S_1 \rightarrow S_0$  radiative rate constant, congruent with the Strickler–Berg relationship [22]; most strongly absorbing organic NIR dyes, however, are not impressive emitters, due in many cases to large magnitude  $S_1$  state non-radiative rate constants that are readily rationalized within the context of the energy gap law [23].

Porphyrins are tetrapyrrole  $\pi$ -conjugated systems, and the lowest energy absorption bands of simple tetraphenylporphyrin or octaethylporphyrin monomers range typically over the 600 to 650 nm spectral regime and feature modest absorptive extinction coefficients ( $\epsilon < 10^4 \text{ M}^{-1} \cdot \text{cm}^{-1}$ ). Modification of the porphyrin  $\pi$ -skeleton can further reduce the HOMO–LUMO gap; the electronic structures of such reduced band gap porphyrins can in general be rationalized using Gouterman's four orbital model [24]. In a simple (porphinato)metal complex having  $D_{4h}$  symmetry, the LUMO is doubly degenerate, and the HOMO and HOMO-1 are nearly degenerate in energy; as a result, substantial configuration interaction mixes the ( $a_{1u} \rightarrow e_g$ ) and ( $a_{2u} \rightarrow e_g$ ) transitions. Constructive and destructive combinations of these one-electron transitions give rise to an intense shorter-wavelength Soret band and a weakly absorbing longer-wavelength Q-band. While removal of frontier orbital (HOMO/HOMO-1, LUMO/LUMO+1) degeneracy is expected to result in augmentation of the Q-band absorptive extinction coefficient, relatively few examples exist of low band gap porphyrin derivatives that possess intense NIR Q-bands [25–29].

In contrast, the chlorophylls, natural porphyrin derivatives, possess lowest energy Q-bands with significant extinction coefficients ( $\epsilon: 0.5 \sim 1 \times 10^5 \text{ M}^{-1} \cdot \text{cm}^{-1}$ ) [30, 31]; some chlorophyll derivatives and related macrocycles feature substantial fluorescence quantum yields that range from  $\sim 0.05$  to  $0.3$  [32, 33]. While significant strides have been made in recent years regarding chlorophyll synthesis [33–35], the more involved nature of their fabrication limits many possible applications of these structures. Chromophores within the phthalocyanine family also exhibit intense low energy electronic absorption bands ( $\epsilon: 1 \sim 2 \times 10^5 \text{ M}^{-1} \cdot \text{cm}^{-1}$ ); while a few examples of these chromophores are known that feature both substantial NIR absorptivity and significant fluorescence quantum yield ( $0.1 \sim 0.8$ ) [36, 37], it is important to point out that extensive modulation of phthalocyanine absorptive properties and photophysics is limited by the modest frontier orbital electron density localized at the periphery of the macrocycle-fused benzene rings [38].

We have explored synthesis and electronic properties of *meso*-ethynyl porphyrin derivatives [39–62] for nonlinear optics [60, 63–81], optoelectronic devices [82–87], and fluorescence-based optical imaging technologies [88–97].

Ethyne groups fused to the porphyrin *meso*-positions provide significant electronic interaction with the macrocycle  $a_{2u}$ -derived HOMO and remove the degeneracy of the low-lying empty  $e_g$  orbitals [39, 42, 45, 50, 55]. Here we report the synthesis and optical properties of conjugated 5,15-diethynyl(porphinato)zinc(II) complexes that feature conjugated terminal groups having varying degrees of proquinoidal character (Fig. 1) that drive intense Q-band absorptions; the uncommon emissive properties of these new fluorophores based on a (5,15-diethynylporphinato) zinc(II) framework are discussed within the context of the Strickler–Berg relationship.

## EXPERIMENTAL

### Materials

All manipulations were carried out under nitrogen previously passed through an  $O_2$  scrubbing tower (Schweitzerhall R3-11 catalyst) and a drying tower (Linde 3-Å molecular sieves) unless otherwise stated. Air sensitive solids were handled in a Braun 150-M glove box. Standard Schlenk techniques were employed to manipulate air-sensitive solutions. Tetrahydrofuran (THF) was distilled from K/4-benzoylbiphenyl under  $N_2$ . Triethylamine and MeOH were distilled from  $CaH_2$  under  $N_2$ . The catalysts  $Pd(PPh_3)_4$ ,  $Pd(PPh_3)_2Cl_2$ , dichloro[1,1'-bis(diphenylphosphino)ferrocene]palladium(II) dichloromethane adduct,  $P(t-Bu)_3$  (10 wt% solution in hexanes), tris(dibenzylideneacetone)dipalladium(0) ( $Pd_2dba_3$ ), CuI and triphenylarsine ( $AsPh_3$ ) were purchased from Strem Chemicals and used as received. 4-Bromobenzo[c][1,2,5]thiadiazole, and 4,7-dibromobenzo[c][1,2,5]thiadiazole were prepared by literature methods [98]. (5,15-Bis[trimethylsilylethynyl]-10,20-bis[3',5'-bis(9"-methoxy-1",4",7"-trioxanonyl)phenyl]porphinato)zinc(II) (1), (5,15-dibromo-10,20-bis[2',6'-bis(3",3"-dimethyl-1"-butyloxy)phenyl]porphinato)zinc(II), (5,15-diethynyl-10,20-bis[2',6'-bis(3",3"-dimethyl-1"-butyloxy)phenyl]porphinato)zinc(II), and (5,15-bis(4'-(*N,N*-dimethylamino)phenylethynyl)-10,20-bis[2',6'-bis(3",3"-dimethyl-1"-butyloxy)phenyl]porphinato)zinc(II) (2) were synthesized as described previously [50, 54, 66]. A number of key precursors were synthesized as reported earlier [99]. All NMR solvents, and all other chemicals, were used as received.

Chemical shifts for  $^1H$  NMR spectra are relative to the tetramethylsilane (TMS) signal in deuterated solvent (TMS,  $\delta = 0.00$  ppm). All  $J$  values are reported in Hertz. Flash and size exclusion column chromatography were performed on the bench top, using respectively silica gel (EM Science, 230–400 mesh) and Bio-Rad Bio-Beads SX-1 as media. CI mass spectra were acquired at the Mass Spectrometry Center at the University of Pennsylvania. MALDI-TOF mass spectroscopic data were obtained with a Voyager-DE RP instrument

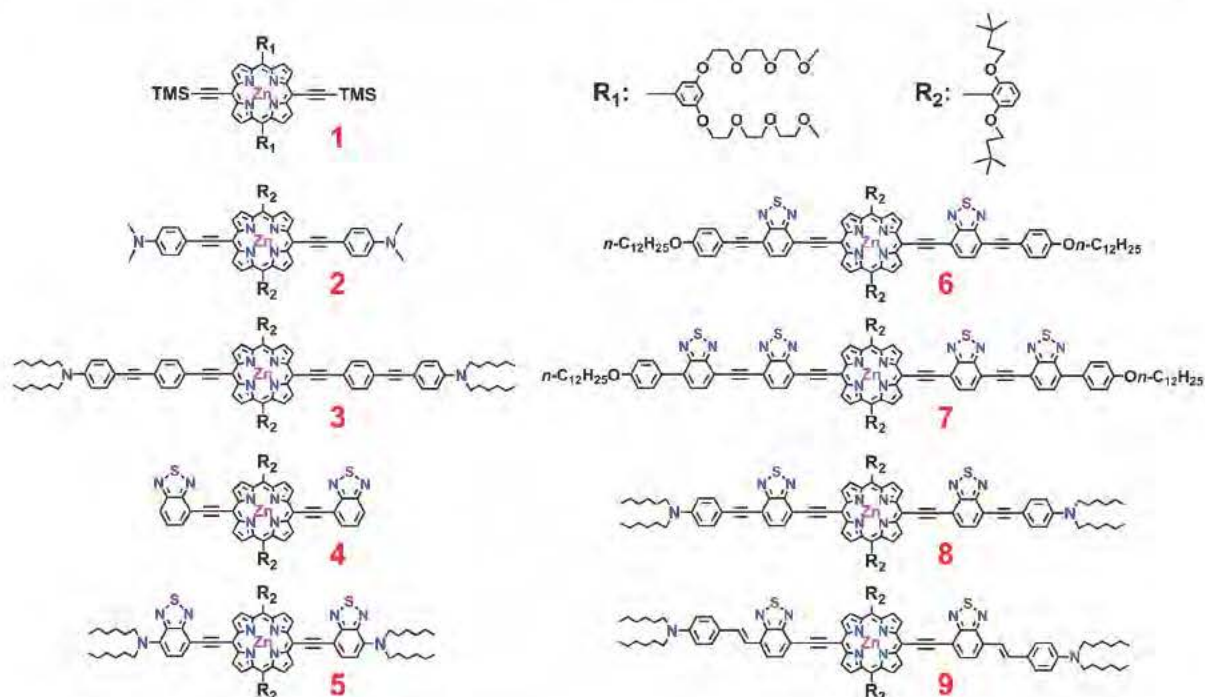


Fig. 1. Structures of the TMS-protected (5,15-diethynyl-10,20-bis[3',5'-bis(9''-methoxy-1'',4'',7''-trioxanonyl)phenyl]porphinato) zinc(II) reference monomer (1), and NIR fluorophores 2–9

(PerSeptive Biosystems); samples for these experiments were prepared as micromolar solutions in either CH<sub>2</sub>Cl<sub>2</sub> or THF, and dithranol (Sigma–Aldrich) was utilized as the matrix.

### Instrumentation

<sup>1</sup>H NMR spectra were recorded on either 250 MHz AC-250, 300 MHz DMX-300, or 500 MHz AMX-500 Bruker spectrometers. Electronic absorption spectra were recorded on a Shimadzu PharmaSpec UV1700 spectrophotometer. Fluorescence spectra were obtained with a Spex Fluorolog-3 spectrophotometer (Jobin Yvon Inc., Edison, NJ) that utilized a T-channel configuration with red sensitive R2658 Hamamatsu PMT and liquid nitrogen cooled InGaAs detectors. The obtained fluorescence spectra were corrected using the spectral output of a calibrated light source supplied by the National Bureau of Standards. Fluorescence quantum yields were measured on N<sub>2</sub>-purged solutions at room temperature. Tetraphenylporphyrin in benzene ( $\Phi_f = 0.13$ ) was used as a standard [100]. The fluorescence quantum yields of each sample were calculated using the following equation (Equation 1)

$$\frac{\Phi_{f(s)}}{\Phi_{f(r)}} = \frac{F_s \cdot A_r \cdot n_s^2}{F_r \cdot A_s \cdot n_r^2} \quad (1)$$

where  $\Phi_f$  is the fluorescence quantum yield,  $F$  is the area under the corrected fluorescence band (expressed

in number of photons),  $A$  is the absorbance at the excitation wavelength, and  $n$  is the refractive index of the solvents used. Subscripts  $s$  and  $r$  refer to the sample and reference, respectively. Time-correlated single-photon counting (TCSPC) experiments to measure fluorescence lifetimes were performed using an Edinburgh Analytical Instruments FL/FS 900 spectrofluorimeter. The excitation sources for TCSPC measurements were either a nanosecond flash lamp operating under an atmosphere of H<sub>2</sub> gas (0.50–0.55 bar, 0.7 nm fwhm, 40 kHz repetition rate) or a blue (450 ± 15 nm) light-emitting diode (Picoquant PLS 450/PDL 800-B) triggered at a frequency of 100 kHz by a Berkeley Nucleonics 555 pulse generator. TCSPC data were analyzed by iterative convolution of the fluorescence decay profile with the instrument response function using software provided by Edinburgh Instruments.

### Synthesis

(5,15-Bis[4'-(4''-*N,N*-dihexylaminophenylethynyl)phenylethynyl]-10,20-bis[2',6'-bis(3'',3''-dimethyl-1''-butyloxy)phenyl]porphinato)zinc(II) (3). 1-(4'-*N,N*-dihexylaminophenylethynyl)-4-iodobenzene [99] (55.5 mg, 1.14 × 10<sup>-4</sup> mol), (5,15-diethynyl-10,20-bis[2',6'-bis(3'',3''-dimethyl-1''-butyloxy)phenyl]porphinato)zinc(II) (50.4 mg, 5.17 × 10<sup>-5</sup> mol), Pd(PPh<sub>3</sub>)<sub>4</sub> (13.2 mg, 1.14 × 10<sup>-5</sup> mol), CuI (1.0 mg, 5.3 × 10<sup>-6</sup> mol) and dry THF (7.0 mL) were added to a 100-mL round-bottom flask. Ar was bubbled into the reaction mixture for 5 min before

piperidine (0.50 mL) was added. The reaction mixture was stirred at 45 °C for 3.5 h under Ar. After the solvent was evaporated, the residue was chromatographed on silica gel with 8:1 hexanes:THF as the eluent. Yield 0.063 g (72% based on 50.4 mg of (5,15-diethynyl-10,20-bis[2',6'-bis(3'',3''-dimethyl-1''-butyloxy)phenyl]porphinato)zinc(II)). <sup>1</sup>H NMR (300 MHz; CDCl<sub>3</sub>): δ, ppm 9.67 (d, 4H, *J* = 4.6 Hz, β-H), 8.86 (d, 4H, *J* = 4.6 Hz, β-H), 7.96 (d, 4H, *J* = 8.4 Hz, Ph-H), 7.72 (t, 2H, *J* = 8.4 Hz, Ph-H), 7.65 (d, 4H, *J* = 8.4 Hz, Ph-H), 7.43 (d, 4H, *J* = 8.8 Hz, Ph-H), 7.02 (d, 4H, *J* = 8.5 Hz, Ph-H), 6.61 (d, 2H, *J* = 9.0 Hz, Ph-H), 3.92 (t, 8H, *J* = 7.3 Hz, -O-CH<sub>2</sub>-C), 3.30 (t, 8H, *J* = 7.6 Hz, -N-CH<sub>2</sub>-C), 1.60 (m, 8H, -N-C-CH<sub>2</sub>-C), 1.2-1.4 (m, 24H, -CH<sub>2</sub>-), 0.92 (t, 8H, *J* = 6.8 Hz, O-C-CH<sub>2</sub>-), 0.89 (t, 12H, *J* = 7.3 Hz, -CH<sub>3</sub>), 0.27 (s, 36H, -C-CH<sub>3</sub>). MS (MALDI-TOF): *m/z* 1690.92 (calcd. for [M]<sup>+</sup> 1690.976).

**4-(Trimethylsilylethynyl)benzo[c][1,2,5]thiadiazole.** 4-Bromobenzo[c][1,2,5]thiadiazole (0.378 g, 1.76 × 10<sup>-3</sup> mol), Pd(PPh<sub>3</sub>)<sub>4</sub> (0.125 g, 1.08 × 10<sup>-4</sup> mol), CuI (14 mg, 7.4 × 10<sup>-5</sup> mol) and dry THF (20 mL) were added to a 100-mL round-bottom flask. Ar was bubbled into the reaction mixture for 5 min before diisopropylamine (1.0 mL) and (trimethylsilyl)acetylene (1.00 mL, 7.1 × 10<sup>-3</sup> mol) were added. The reaction mixture was stirred at 45 °C for 11 h under Ar. After cooling, the solvent was evaporated. The residue was chromatographed on silica gel column with 1:1 hexanes:CHCl<sub>3</sub> as the eluent. Yield 0.406 g (99% based on 0.378 g of 4-bromobenzo[c][1,2,5]thiadiazole). <sup>1</sup>H NMR (300 MHz; CDCl<sub>3</sub>): δ, ppm 7.99 (dd, 1H, *J* = 1.0, 8.8 Hz, Ph-H), 7.77 (dd, 1H, *J* = 1.0, 7.0 Hz, Ph-H), 7.55 (dd, 1H, *J* = 7.0, 8.8 Hz, Ph-H), 0.34 (s, 9H, -Si-CH<sub>3</sub>). MS (CI): *m/z* 232.048 (calcd. for [M]<sup>+</sup> 232.049).

**4-Ethynylbenzo[c][1,2,5]thiadiazole.** 4-(Trimethylsilylethynyl)benzo[c][1,2,5]thiadiazole (0.100 g, 4.30 × 10<sup>-4</sup> mol), K<sub>2</sub>CO<sub>3</sub> (78.6 mg, 5.7 × 10<sup>-4</sup> mol), THF (3.0 mL), and MeOH (2.0 mL) were added to a 100-mL round-bottom flask. The reaction mixture was stirred at room temperature for 1.5 h under Ar. The reaction mixture was filtered and the solvent was evaporated. Yield quantitative. <sup>1</sup>H NMR (300 MHz; CDCl<sub>3</sub>): δ, ppm 8.04 (d, 1H, *J* = 8.8 Hz, Ph-H), 7.81 (d, 1H, *J* = 6.9 Hz, Ph-H), 7.58 (t, 1H, *J* = 8.0 Hz, Ph-H), 3.59 (s, 1H, ethynyl-H). MS (CI): *m/z* 160.009 (calcd. for [M]<sup>+</sup> 160.010).

**(5,15-Bis(benzo[c][1,2,5]thiadiazol-4-ylethynyl)-10,20-bis[2',6'-bis(3'',3''-dimethyl-1''-butyloxy)phenyl]-porphinato)zinc(II) (4).** 4-Ethynylbenzo[c][1,2,5]thiadiazole (40.0 mg, 2.50 × 10<sup>-4</sup> mol), (5,15-dibromo-10,20-bis[2',6'-bis(3'',3''-dimethyl-1''-butyloxy)phenyl]porphinato)zinc(II) (71.0 mg, 2.50 × 10<sup>-4</sup> mol), Pd(PPh<sub>3</sub>)<sub>4</sub> (22.6 mg, 2.0 × 10<sup>-5</sup> mol), CuI (2.0 mg, 1.1 × 10<sup>-5</sup> mol) and dry THF (10 mL) were added to a 100-mL round-bottom flask. Ar was bubbled into the reaction mixture for 5 min before piperidine (0.50 mL) was added. The reaction mixture was stirred at 48 °C for 24 h under Ar. After cooling, the solvent was evaporated. The

residue was chromatographed on silica gel column with 5:1 hexanes:THF as the eluent. The product was further purified by size exclusion column chromatography (Bio Rad Bio-Beads SX-1 packed in THF, gravity flow). Yield 40.7 mg (50% based on 71.0 mg of (5,15-dibromo-10,20-bis[2',6'-bis(3'',3''-dimethyl-1''-butyloxy)phenyl]porphinato)zinc(II)). <sup>1</sup>H NMR (300 MHz; CDCl<sub>3</sub>): δ, ppm 9.91 (d, 4H, *J* = 4.5 Hz, β-H), 8.87 (d, 4H, *J* = 4.5 Hz, β-H), 8.18 (d, 2H, *J* = 7.0 Hz, Ph-H), 8.07 (d, 2H, *J* = 8.8 Hz, Ph-H), 7.76 (dd, 2H, *J* = 7.0, 8.8 Hz, Ph-H), 7.72 (t, 2H, *J* = 8.4 Hz, Ph-H), 7.03 (d, 4H, *J* = 8.4 Hz, Ph-H), 3.92 (t, 8H, *J* = 7.6 Hz, -O-CH<sub>2</sub>-C), 0.83 (t, 8H, *J* = 7.5 Hz, -O-C-CH<sub>2</sub>-C), 0.37 (s, 36H, -C-CH<sub>3</sub>). MS (MALDI-TOF): *m/z* 1240.7 (calcd. for [M]<sup>+</sup> 1240.441).

**(5,15-Bis[4'-(*N,N*-dihexylamino)benzo[c][1',2',5']thiadiazole-7'-ylethynyl]-10,20-bis[2',6'-bis(3'',3''-dimethyl-1''-butyloxy)phenyl]porphinato)zinc(II) (5).** 4-Bromo-7-(*N,N*-dihexylamino)benzo[c][1,2,5]thiadiazole [99] (53.8 mg, 1.35 × 10<sup>-4</sup> mol), (5,15-diethynyl-10,20-bis[2',6'-bis(3'',3''-dimethyl-1''-butyloxy)phenyl]porphinato)zinc(II) (41.0 mg, 4.2 × 10<sup>-5</sup> mol), Pd(PPh<sub>3</sub>)<sub>4</sub> (12.8 mg, 1.1 × 10<sup>-5</sup> mol), CuI (1.1 mg, 5.8 × 10<sup>-6</sup> mol) and dry THF (5.0 mL) were added to a 100-mL round-bottom flask. Ar was bubbled into the reaction mixture for 5 min before piperidine (0.20 mL) was added. The reaction mixture was stirred at 45 °C for 24 h under Ar. After the solvent was evaporated, the residue was chromatographed on silica gel with 8:1 hexanes: THF as the eluent. Yield 22.0 mg (33% based on 41.0 mg of (5,15-diethynyl-10,20-bis[2',6'-bis(3'',3''-dimethyl-1''-butyloxy)phenyl]porphinato)zinc(II)). <sup>1</sup>H NMR (300 MHz; CDCl<sub>3</sub>): δ, ppm 9.94 (d, 4H, *J* = 4.6 Hz, β-H), 8.86 (d, 4H, *J* = 4.6 Hz, β-H), 8.07 (d, 2H, *J* = 8.2 Hz, Ph-H), 7.70 (t, 2H, *J* = 8.4 Hz, Ph-H), 7.00 (d, 4H, *J* = 8.5 Hz, Ph-H), 6.59 (d, 2H, *J* = 8.3 Hz, Ph-H), 3.91 (t, 8H, *J* = 7.2 Hz, -O-CH<sub>2</sub>-C), 3.86 (t, 8H, *J* = 8.3 Hz, -N-CH<sub>2</sub>-C), 1.79 (m, 8H, -N-C-CH<sub>2</sub>-C), 1.1-1.5 (m, 24H, -CH<sub>2</sub>-), 0.94 (t, 8H, *J* = 7.0 Hz, O-C-CH<sub>2</sub>-), 0.88 (t, 12H, *J* = 7.2 Hz, -CH<sub>3</sub>), 0.26 (s, 36H, -C-CH<sub>3</sub>). MS (MALDI-TOF): *m/z* 1607.08 (calcd. for [M]<sup>+</sup> 1606.838).

**4-Bromo-7-(4'-*n*-dodecyloxyphenylethynyl)benzo[c][1,2,5]thiadiazole.** 4-*n*-Dodecyloxyethynylbenzene [99] (0.620 g, 2.16 × 10<sup>-3</sup> mol), 4,7-dibromobenzo[c][1,2,5]thiadiazole (1.91 g, 6.50 × 10<sup>-3</sup> mol), Pd(PPh<sub>3</sub>)<sub>2</sub>Cl<sub>2</sub> (0.162 g, 2.31 × 10<sup>-4</sup> mol), CuI (21 mg, 1.1 × 10<sup>-4</sup> mol), and dry toluene (10 mL) were added to a 100-mL round-bottom flask. Ar was bubbled into the reaction mixture for 5 min before triethylamine (10 mL) was added. The reaction mixture was stirred at 45 °C for 3 h under Ar. After the solvent was evaporated, the reaction mixture was chromatographed on silica gel with 2:1 hexanes:CH<sub>2</sub>Cl<sub>2</sub>. Yield 0.496 g (46% based on 0.620 g of 4-*n*-dodecyloxyethynylbenzene). <sup>1</sup>H NMR (300 MHz; CDCl<sub>3</sub>): δ, ppm 7.83 (d, 1H, *J* = 7.6 Hz, Ph-H), 7.63 (d, 1H, *J* = 7.6 Hz, Ph-H), 7.59 (d, 2H, *J* = 8.9 Hz, Ph-H), 6.91 (d, 2H, *J* = 8.9 Hz, Ph-H), 3.99 (t, 2H, *J* = 6.6 Hz, -OCH<sub>2</sub>-), 1.80 (quint, 2H, -OC-CH<sub>2</sub>-), 1.45 (m, 2H,

–CH<sub>2</sub>–), 1.2–1.4 (m, 16H, –CH<sub>2</sub>–), 0.88 (t, 3H, *J* = 6.7 Hz, –CH<sub>3</sub>). MS (CI): *m/z* 498.133 (calcd. for [M]<sup>+</sup> 498.134).

**(5,15-Bis([7'-(4'-*n*-dodecyloxyphenylethynyl)benzo[c][1,2,5]thiadiazol-4'-yl]ethynyl)-10,20-bis[2',6'-bis(3'',3''-dimethyl-1''-butyloxy)phenyl]porphinato)zinc(II) (6).** 4-Bromo-7-(4'-*n*-dodecyloxyphenylethynyl)benzo[c][1,2,5]thiadiazole (40.9 mg, 8.19 × 10<sup>−5</sup> mol), (5,15-diethynyl-10,20-bis[2',6'-bis(3'',3''-dimethyl-1''-butyloxy)phenyl]porphinato)zinc(II) (35.7 mg, 3.66 × 10<sup>−5</sup> mol), Pd(PPh<sub>3</sub>)<sub>4</sub> (10.1 mg, 8.7 × 10<sup>−6</sup> mol), CuI (1.3 mg, 6.8 × 10<sup>−6</sup> mol), and dry THF (6.0 mL) were added to a 100-mL round-bottom flask. Ar was bubbled into the reaction mixture for 10 min before piperidine (0.50 mL) was added. The reaction mixture was stirred at 44 °C for 17.5 h under Ar. After cooling, the solvent was evaporated. The residue was chromatographed on silica gel with 5:1 hexanes:THF as the eluent. The product was further purified by size exclusion column chromatography (BioRad Bio-Beads SX-1 packed in THF, gravity flow). Yield 45.5 mg (69% based on 35.7 mg of 5,15-diethynyl-10,20-bis[2',6'-bis(3'',3''-dimethyl-1''-butyloxy)phenyl]porphinato)zinc(II)). <sup>1</sup>H NMR (300 MHz; 1 drop pyridine-*d*<sub>5</sub> in CDCl<sub>3</sub>): δ, ppm 9.90 (d, 4H, *J* = 4.6 Hz, β-H), 8.86 (d, 4H, *J* = 4.6 Hz, β-H), 8.15 (d, 2H, *J* = 7.4 Hz, Ph-H), 7.92 (d, 2H, *J* = 7.4 Hz, Ph-H), 7.72 (t, 2H, *J* = 8.4 Hz, Ph-H), 7.65 (d, 4H, *J* = 8.8 Hz, Ph-H), 7.03 (d, 4H, *J* = 8.5 Hz, Ph-H), 6.94 (d, 4H, *J* = 8.9 Hz, Ph-H), 4.01 (t, 4H, *J* = 6.6 Hz, –O–CH<sub>2</sub>–C), 3.93 (t, 8H, *J* = 7.5 Hz, –O–CH<sub>2</sub>–C), 1.82 (quint, 4H, *J* = 6.8 Hz, –O–CH<sub>2</sub>–C), 1.48 (m, 4H, –CH<sub>2</sub>–), 1.15–1.40 (m, 32H, –CH<sub>2</sub>–), 0.89 (t, 6H, *J* = 6.7 Hz, –CH<sub>3</sub>), 0.83 (t, 8H, *J* = 7.5 Hz, –OC–CH<sub>2</sub>–), 0.37 (s, 36H, –C–CH<sub>3</sub>). MS (MALDI-TOF): *m/z* 1809.0 (calcd. for [M]<sup>+</sup> 1808.869).

**4-*n*-Dodecyloxyphenyl-4',4',5',5'-tetramethyl-1',3',2'-dioxaborolane.** 4-*n*-Dodecyloxyiodobenzene [99] (1.00 g, 2.58 × 10<sup>−3</sup> mol), dichloro[1,1'-bis(diphenylphosphino)ferrocene]palladium(II)-dichloromethane adduct (0.106 g, 1.30 × 10<sup>−4</sup> mol) were added to 1,2-dichloroethane (5.0 mL) and Et<sub>3</sub>N (1.0 mL, 7.2 × 10<sup>−3</sup> mol). 4,4,5,5-Tetramethyl-1,3,2-dioxaborolane (0.56 mL, 3.9 × 10<sup>−3</sup> mol) was added, and the reaction mixture was stirred at 75 °C for 1.5 h under Ar. After cooling, the solvent was evaporated. The residue was chromatographed on silica gel with 2:1 hexanes:CHCl<sub>3</sub> as the eluent. Yield 0.674 g (67% based on 1.00 g of 4-*n*-dodecyloxyiodobenzene). <sup>1</sup>H NMR (250 MHz; CDCl<sub>3</sub>): δ, ppm 7.73 (d, 2H, *J* = 8.7 Hz, Ph-H), 6.88 (d, 2H, *J* = 8.7 Hz, Ph-H), 3.97 (t, 2H, *J* = 6.6 Hz, –OCH<sub>2</sub>–), 1.78 (quint, 2H, *J* = 6.6 Hz, –OC–CH<sub>2</sub>–), 1.45 (m, 2H, –CH<sub>2</sub>–), 1.33 (s, 12H, –CH<sub>3</sub>), 1.26 (m, 16H, –CH<sub>2</sub>–), 0.88 (t, 3H, *J* = 6.5 Hz, –CH<sub>3</sub>). MS (CI): *m/z* 388.317 (calcd. for [M]<sup>+</sup> 388.315).

**4-Bromo-7-(4'-*n*-dodecyloxyphenyl)benzo[c][1,2,5]thiadiazole.** 4-*n*-Dodecyloxyphenyl-4',4',5',5'-tetramethyl-1',3',2'-dioxaborolane (0.313 g, 8.06 × 10<sup>−4</sup> mol), 4,7-dibromobenzo[c][1,2,5]thiadiazole (0.474 g, 1.61 × 10<sup>−3</sup> mol), Pd(PPh<sub>3</sub>)<sub>4</sub> (97 mg, 8.4 × 10<sup>−5</sup> mol), K<sub>2</sub>CO<sub>3</sub>

(0.347 g, 2.51 × 10<sup>−3</sup> mol), DMF (25 mL), and H<sub>2</sub>O (3.0 mL) were added to a 100-mL round-bottom flask. Ar was bubbled into the reaction mixture for 5 min at room temperature. The reaction mixture was warmed up to 86 °C and stirred for 7.5 h under Ar. After cooling, 200 mL of dilute aq. HCl was added to the reaction mixture, and the product was extracted with CHCl<sub>3</sub> and dried over Na<sub>2</sub>SO<sub>4</sub>. The solvent was evaporated, and the residue was chromatographed on silica gel with 1:1 hexanes:CHCl<sub>3</sub>. The product was further purified by size exclusion column chromatography (BioRad Bio-Beads SX-1 packed in THF, gravity flow). Yield 0.295 g (77% based on 0.313 g of 4-*n*-dodecyloxyphenyl-4',4',5',5'-tetramethyl-1',3',2'-dioxaborolane). <sup>1</sup>H NMR (300 MHz; CDCl<sub>3</sub>): δ, ppm 7.90 (d, 1H, *J* = 7.6 Hz, –CH<sub>2</sub>–), 7.85 (d, 2H, *J* = 8.8 Hz, Ph-H), 7.53 (d, 1H, *J* = 7.6 Hz, Ph-H), 7.05 (d, 2H, *J* = 8.8 Hz, Ph-H), 4.04 (t, 2H, *J* = 6.5 Hz, –OCH<sub>2</sub>–), 1.83 (quint, 2H, *J* = 6.5 Hz, –OC–CH<sub>2</sub>–), 1.49 (m, 2H, –CH<sub>2</sub>–), 1.2–1.4 (m, 16H, –CH<sub>2</sub>–), 0.88 (t, 3H, *J* = 6.6 Hz, –CH<sub>3</sub>). MS (CI): *m/z* 474.133 (calcd. for [M]<sup>+</sup> 474.134).

**4-(4'-*n*-Dodecyloxyphenyl)-7-(trimethylsilyl-ethynyl)benzo[c][1,2,5]thiadiazole.** 4-Bromo-7-(4'-*n*-dodecyloxyphenyl)benzo[c][1,2,5]thiadiazole (0.2364 g, 4.97 × 10<sup>−4</sup> mol), Pd(PPh<sub>3</sub>)<sub>4</sub> (55.4 mg, 4.79 × 10<sup>−5</sup> mol), CuI (3.4 mg, 1.8 × 10<sup>−5</sup> mol), and dry THF (10 mL) were added to a 100-mL round-bottom flask. Ar was bubbled into the reaction mixture for 5 min before (trimethylsilyl)acetylene (0.25 mL, 1.8 × 10<sup>−3</sup> mol) and diisopropylamine (1.0 mL) were added. The reaction mixture was stirred at 50 °C for 17.5 h under Ar. After cooling, the solvent was evaporated. The residue was chromatographed on silica gel with 8:1 hexanes:THF. Yield 0.240 g (98% based on 0.2364 g of 4-bromo-7-(4'-*n*-dodecyloxyphenyl)benzo[c][1,2,5]thiadiazole). <sup>1</sup>H NMR (300 MHz; CDCl<sub>3</sub>): δ, ppm 7.90 (d, 2H, *J* = 8.9 Hz, Ph-H), 7.82 (d, 1H, *J* = 7.4 Hz, Ph-H), 7.61 (d, 1H, *J* = 7.4 Hz, Ph-H), 7.05 (d, 2H, *J* = 8.9 Hz, Ph-H), 4.04 (t, 2H, *J* = 6.5 Hz, –OCH<sub>2</sub>–), 1.82 (quint, 2H, *J* = 6.9 Hz, –OC–CH<sub>2</sub>–), 1.49 (m, 2H, –CH<sub>2</sub>–), 1.2–1.4 (m, 16H, –CH<sub>2</sub>–), 0.88 (t, 3H, *J* = 6.7 Hz, –CH<sub>3</sub>), 0.34 (s, 9H, –Si–CH<sub>3</sub>). MS (CI): *m/z* 493.272 (calcd. for [M + H]<sup>+</sup> 493.271).

**4-(4'-*n*-Dodecyloxyphenyl)-7-ethynylbenzo[c][1,2,5]thiadiazole.** 4-(4'-*n*-Dodecyloxyphenyl)-7-(trimethylsilyl-ethynyl)benzo[c][1,2,5]thiadiazole (0.223 g, 4.53 × 10<sup>−4</sup> mol) was dissolved in a mixture of THF (7.0 mL) and MeOH (3.0 mL). K<sub>2</sub>CO<sub>3</sub> (85 mg, 6.2 × 10<sup>−4</sup> mol) was added, and the reaction mixture was stirred for 2 h under Ar. The reaction mixture was filtered and the filtrate evaporated. Yield 0.190 g (99.7% based on 0.223 g of 4-(4'-*n*-dodecyloxyphenyl)-7-(trimethylsilyl-ethynyl)benzo[c][1,2,5]thiadiazole). <sup>1</sup>H NMR (300 MHz; CDCl<sub>3</sub>): δ, ppm 7.90 (d, 2H, *J* = 8.9 Hz, Ph-H), 7.86 (d, 1H, *J* = 7.3 Hz, Ph-H), 7.63 (d, 1H, *J* = 7.4 Hz, Ph-H), 7.06 (d, 2H, *J* = 8.9 Hz, Ph-H), 4.04 (t, 2H, *J* = 6.5 Hz, –OCH<sub>2</sub>–), 3.60 (s, 1H, ethynyl-H), 1.83 (quint, 2H,

$J = 6.9$  Hz,  $-\text{OC}-\text{CH}_2-$ ), 1.49 (m, 2H,  $-\text{CH}_2-$ ), 1.2–1.4 (m, 16H,  $-\text{CH}_2-$ ), 0.88 (t, 3H,  $J = 6.7$  Hz,  $-\text{CH}_3$ ). MS (ESI):  $m/z$  421.233 (calcd. for  $[\text{M} + \text{H}]^+$  421.231).

**4-([4'-(4''-*n*-Dodecyloxyphenyl)benzo[c][1',2',5']thiadiazol-7'-yl)ethynyl)-7-iodobenzo[c][1,2,5]thiadiazole.** 4-(4'-*n*-Dodecyloxyphenyl)-7-ethynylbenzo[c][1,2,5]thiadiazole (0.120 g,  $2.85 \times 10^{-4}$  mol), 4,7-diiodobenzo[c][1,2,5]thiadiazole [99] (0.232 g,  $5.98 \times 10^{-4}$  mol),  $\text{Pd}_2\text{dba}_3$  (32.8 mg,  $3.6 \times 10^{-5}$  mol),  $\text{AsPh}_3$  (92.4 mg,  $3.0 \times 10^{-4}$  mol), and dry THF (15 mL) were added to a 100-mL round-bottom flask. Ar was bubbled into the reaction mixture for 5 min before diisopropylethylamine (1.0 mL) was added. The reaction mixture was stirred at 48 °C for 12.5 h under Ar. After cooling, the solvent was evaporated. The residue was chromatographed on silica gel with 8:1 hexanes:THF. The product was further purified by size exclusion column chromatography (BioRad Bio-Beads SX-1 packed in THF, gravity flow). Yield 69.8 mg (36% based on 0.120 g of 4-(4'-*n*-dodecyloxyphenyl)-7-ethynylbenzo[c][1,2,5]thiadiazole).  $^1\text{H}$  NMR (300 MHz;  $\text{CDCl}_3$ ):  $\delta$ , ppm 8.16 (d, 1H,  $J = 7.5$  Hz, Ph-H), 8.03 (d, 1H,  $J = 7.4$  Hz, Ph-H), 7.96 (d, 2H,  $J = 8.9$  Hz, Ph-H), 7.71 (d, 1H,  $J = 7.4$  Hz, Ph-H), 7.70 (d, 1H,  $J = 7.5$  Hz, Ph-H), 7.08 (d, 2H,  $J = 8.9$  Hz, Ph-H), 4.05 (t, 2H,  $J = 6.5$  Hz,  $-\text{OCH}_2-$ ), 1.84 (quint, 2H,  $J = 7.0$  Hz,  $-\text{OC}-\text{CH}_2-$ ), 1.49 (m, 2H,  $-\text{CH}_2-$ ), 1.2–1.4 (m, 16H,  $-\text{CH}_2-$ ), 0.88 (t, 3H,  $J = 6.6$  Hz,  $-\text{CH}_3$ ). MS (MALDI-TOF):  $m/z$  680.09 (calcd. for  $[\text{M}]^+$  680.110).

**5,15-Bis([7'-([7''-(4'''-*n*-dodecyloxyphenyl)benzo[c][1'',2'',5'']thiadiazol-4'-yl)ethynyl)benzo[c]-[1',2',5']thiadiazol-4'-yl)ethynyl)-10,20-bis[2',6'-bis(3'',3''-dimethyl-1''-butyloxy)phenyl]porphinato)zinc(II) (7).** 4-([4'-(4''-*n*-Dodecyloxyphenyl)benzo[c][1',2',5']thiadiazol-7'-yl)ethynyl)-7-iodobenzo[c][1,2,5]thiadiazole (31.0 mg,  $4.55 \times 10^{-5}$  mol), 5,15-diethynyl-10,20-bis[2',6'-bis(3'',3''-dimethyl-1''-butyloxy)phenyl]porphinato)zinc(II) (22.2 mg,  $2.28 \times 10^{-5}$  mol),  $\text{Pd}(\text{PPh}_3)_4$  (9.1 mg,  $7.9 \times 10^{-6}$  mol),  $\text{CuI}$  (1.7 mg,  $8.9 \times 10^{-6}$  mol), and dry THF (8.0 mL) were added to a 100-mL round-bottom flask. Ar was bubbled into the reaction mixture for 5 min before piperidine (0.50 mL) was added. The reaction mixture was stirred at 50 °C for 3.5 h under Ar. After cooling, the solvent was evaporated. The residue was chromatographed on silica gel with 3:1 hexanes:THF as the eluent. The product was further purified by size exclusion column chromatography (BioRad Bio-Beads SX-1 packed in THF, gravity flow). Yield 30.2 mg (64% based on 31.0 mg of 4-([4'-(4''-*n*-dodecyloxyphenyl)benzo[c][1',2',5']thiadiazol-7'-yl)ethynyl)-7-iodobenzo[c][1,2,5]thiadiazole).  $^1\text{H}$  NMR (300 MHz; 1 drop pyridine- $d_5$  in  $\text{CDCl}_3$ ):  $\delta$ , ppm 9.92 (d, 4H,  $J = 4.6$  Hz,  $\beta$ -H), 8.89 (d, 4H,  $J = 4.5$  Hz,  $\beta$ -H), 8.21 (d, 2H,  $J = 7.4$  Hz, Ph-H), 8.13 (d, 2H,  $J = 7.4$  Hz, Ph-H), 8.09 (d, 2H,  $J = 7.4$  Hz, Ph-H), 7.98 (d, 4H,  $J = 8.7$  Hz, Ph-H), 7.75 (d, 2H,  $J = 7.3$  Hz, Ph-H), 7.73 (t, 2H,  $J = 8.3$  Hz, Ph-H), 7.09 (d, 4H,  $J = 8.8$  Hz, Ph-H), 7.04 (d, 4H,  $J = 8.5$  Hz, Ph-H), 4.06 (t,

4H,  $J = 6.4$  Hz,  $-\text{O}-\text{CH}_2-\text{C}$ ), 3.94 (t, 8H,  $J = 7.5$  Hz,  $-\text{O}-\text{CH}_2-\text{C}$ ), 1.85 (quint, 4H,  $J = 7.0$  Hz,  $-\text{O}-\text{CH}_2-\text{C}$ ), 1.50 (m, 4H,  $-\text{CH}_2-$ ), 1.15–1.40 (m, 32H,  $-\text{CH}_2-$ ), 0.89 (t, 6H,  $-\text{CH}_3$ ), 0.85 (t, 8H,  $J = 7.5$  Hz,  $-\text{OC}-\text{CH}_2-$ ), 0.39 (s, 36H,  $-\text{C}-\text{CH}_3$ ). MS (MALDI-TOF):  $m/z$  2076.99 (calcd. for  $[\text{M}]^+$  2076.857).

**5,15-Bis([7'-([7''-(4'''-*N,N*-dihexylaminophenylethynyl)benzo[c][1',2',5']thiadiazol-4'-yl)ethynyl)-10,20-bis[2',6'-bis(3'',3''-dimethyl-1''-butyloxy)phenyl]porphinato)zinc(II) (8).** 4-(4'-*N,N*-Dihexylaminophenylethynyl)-7-iodobenzo[c][1,2,5]thiadiazole [99] (73.6 mg,  $1.35 \times 10^{-4}$  mol), 5,15-diethynyl-10,20-bis[2',6'-bis(3'',3''-dimethyl-1''-butyloxy)phenyl]porphinato)zinc(II) (59.0 mg,  $6.05 \times 10^{-5}$  mol),  $\text{Pd}(\text{PPh}_3)_4$  (15.6 mg,  $1.35 \times 10^{-5}$  mol),  $\text{CuI}$  (1.0 mg,  $5.3 \times 10^{-6}$  mol), and dry THF (6.0 mL) were added to a 100-mL round-bottom flask. Ar was bubbled into the reaction mixture for 5 min before piperidine (0.50 mL) was added. The reaction mixture was stirred at 49 °C for 20 h under Ar. After cooling, the solvent was evaporated. The residue was chromatographed on silica gel with 5:1 hexanes:THF as the eluent. The product was further purified by size exclusion column chromatography (BioRad Bio-Beads SX-1 packed in THF, gravity flow). Yield 0.107 g (98% based on 59.0 mg of 5,15-diethynyl-10,20-bis[2',6'-bis(3'',3''-dimethyl-1''-butyloxy)phenyl]porphinato)zinc(II)).  $^1\text{H}$  NMR (300 MHz;  $\text{CDCl}_3$ ):  $\delta$ , ppm 9.99 (d, 4H,  $J = 4.6$  Hz,  $\beta$ -H), 8.94 (d, 4H,  $J = 4.6$  Hz,  $\beta$ -H), 8.17 (d, 2H,  $J = 7.4$  Hz, Ph-H), 7.89 (d, 2H,  $J = 7.4$  Hz, Ph-H), 7.73 (t, 2H,  $J = 8.4$  Hz, Ph-H), 7.56 (d, 4H,  $J = 7.7$  Hz, Ph-H), 7.03 (d, 4H,  $J = 8.5$  Hz, Ph-H), 6.64 (d, 4H,  $J = 9.0$  Hz, Ph-H), 3.94 (t, 8H,  $J = 7.3$  Hz,  $-\text{O}-\text{CH}_2-\text{C}$ ), 3.32 (t, 8H,  $J = 7.6$  Hz,  $-\text{N}-\text{CH}_2-\text{C}$ ), 1.5–1.7 (m, 4H,  $-\text{CH}_2-$ ), 1.25–1.45 (m, 24H,  $-\text{CH}_2-$ ), 0.8–1.0 (m, 20H,  $-\text{O}-\text{C}-\text{CH}_2-$  and  $-\text{CH}_3$ ), 0.26 (s, 36H,  $-\text{C}-\text{CH}_3$ ). MS (MALDI-TOF):  $m/z$  1807.1 (calcd. for  $[\text{M}]^+$  1806.901).

**4-(4'-(*N,N*-Dihexylamino)phenylethynyl)-7-iodobenzo[c][1,2,5]thiadiazole.** *N,N*-Dihexylamino-4-vinylbenzene [99] (0.154 g,  $5.36 \times 10^{-4}$  mol), 4,7-diiodobenzo[c][1,2,5]thiadiazole [99] (0.309 g,  $7.96 \times 10^{-4}$  mol),  $\text{Pd}_2\text{dba}_3$  (50.4 mg,  $5.5 \times 10^{-5}$  mol), and dry 1,4-dioxane (7.0 mL) were added to a 100-mL round-bottom flask. Ar was bubbled into the reaction mixture for 5 min before dicyclohexylmethylamine (0.50 mL) and  $\text{P}(\text{t-Bu})_3$  (10 wt% in hexanes, 1.00 mL,  $3.3 \times 10^{-4}$  mol) were added. The reaction mixture was stirred at 57 °C for 48 h under Ar. After the solvent was evaporated, the reaction mixture was chromatographed on silica gel with 8:1 hexanes:THF. The product was further purified by size exclusion column chromatography (BioRad Bio-Beads SX-1 packed in THF, gravity flow). Yield 42.2 mg (14% based on 0.154 g of *N,N*-dihexylamino-4-vinylbenzene).  $^1\text{H}$  NMR (300 MHz;  $\text{CDCl}_3$ ):  $\delta$ , ppm 8.04 (d, 1H,  $J = 7.6$  Hz, Ph-H), 7.84 (d, 1H,  $J = 16.4$  Hz, vinyl-H), 7.50 (d, 2H,  $J = 8.8$  Hz, Ph-H), 7.38 (d, 1H,  $J = 16.2$  Hz, vinyl-H), 7.37 (d, 1H,  $J = 7.8$  Hz, Ph-H), 6.64 (d, 2H,  $J = 8.9$  Hz, Ph-H), 3.30 (t, 4H,  $J = 7.6$  Hz,  $-\text{NCH}_2-$ ), 1.61 (m, 4H,

–NC–CH<sub>2</sub>–), 1.15–1.45 (m, 12H, –CH<sub>2</sub>–), 0.91 (t, 6H, *J* = 6.7 Hz, –CH<sub>3</sub>). MS (CI): *m/z* 547.1481 (calcd. for [M]<sup>+</sup> 547.148).

(5,15-Bis([7'-(4''-*N,N*-dihexylaminophenylethenyl)benzo[c][1',2',5']thiadiazol-4'-yl]ethynyl)-10,20-bis[2',6'-bis(3'',3''-dimethyl-1''-butyloxy)phenyl]porphinato)zinc(II) (**9**). 4-(4'-*N,N*-Dihexylaminophenylethenyl)-7-iodobenzo[c][1,2,5]thiadiazole (42.2 mg, 7.71 × 10<sup>−5</sup> mol), 5,15-diethynyl-10,20-bis[2',6'-bis(3'',3''-dimethyl-1''-butyloxy)phenyl]porphinato)zinc(II) (38.0 mg, 3.90 × 10<sup>−5</sup> mol), Pd(PPh<sub>3</sub>)<sub>4</sub> (10.5 mg, 9.1 × 10<sup>−6</sup> mol), CuI (1.0 mg, 5.3 × 10<sup>−6</sup> mol), and dry THF (5.0 mL) were added to a 100-mL round-bottom flask. Ar was bubbled into the reaction mixture for 5 min before piperidine (0.50 mL) was added. The reaction mixture was stirred at 47 °C for 43 h under Ar. After cooling, the solvent was evaporated. The residue was chromatographed on silica gel with 5:1 hexanes:THF as the eluent. The product was further purified by size exclusion column chromatography (BioRad Bio-Beads SX-1 packed in THF, gravity flow). Yield 30.4 mg (43% based on 42.2 mg of 4-(4'-*N,N*-dihexylaminophenylethenyl)-7-iodobenzo[c][1,2,5]thiadiazole). <sup>1</sup>H NMR (500 MHz; 1 drop pyridine-*d*<sub>5</sub> in CDCl<sub>3</sub>): δ, ppm 9.90 (d, 4H, *J* = 4.5 Hz, β-H), 8.84 (d, 4H, *J* = 4.5 Hz, β-H), 8.14 (d, 2H, *J* = 7.2 Hz, Ph-H), 7.99 (d, 2H, *J* = 16.1 Hz, vinyl-H), 7.77 (d, 2H, *J* = 7.4 Hz, Ph-H), 7.71 (t, 2H, *J* = 8.5 Hz, Ph-H), 7.57 (d, 4H, *J* = 8.4 Hz, Ph-H), 7.55 (d, 2H, *J* = 16.0 Hz, vinyl-H), 7.02 (d, 4H, *J* = 8.6 Hz, Ph-H), 6.68 (d, 4H, *J* = 8.7 Hz, Ph-H), 3.92 (t, 8H, *J* = 7.4 Hz, –O–CH<sub>2</sub>–C), 3.33 (t, 8H, *J* = 7.6 Hz, –N–CH<sub>2</sub>–C), 1.63 (m, 8H, –CH<sub>2</sub>–), 1.3–1.4 (m, 24H, –CH<sub>2</sub>–), 0.93 (t, 12H, *J* = 6.7 Hz, –CH<sub>3</sub>), 0.84 (t, 8H, *J* = 7.5 Hz, –O–C–CH<sub>2</sub>–), 0.39 (s, 36H, –C–CH<sub>3</sub>). MS (MALDI-TOF): *m/z* 1811.0 (calcd. for [M]<sup>+</sup> 1810.932).

## RESULTS AND DISCUSSION

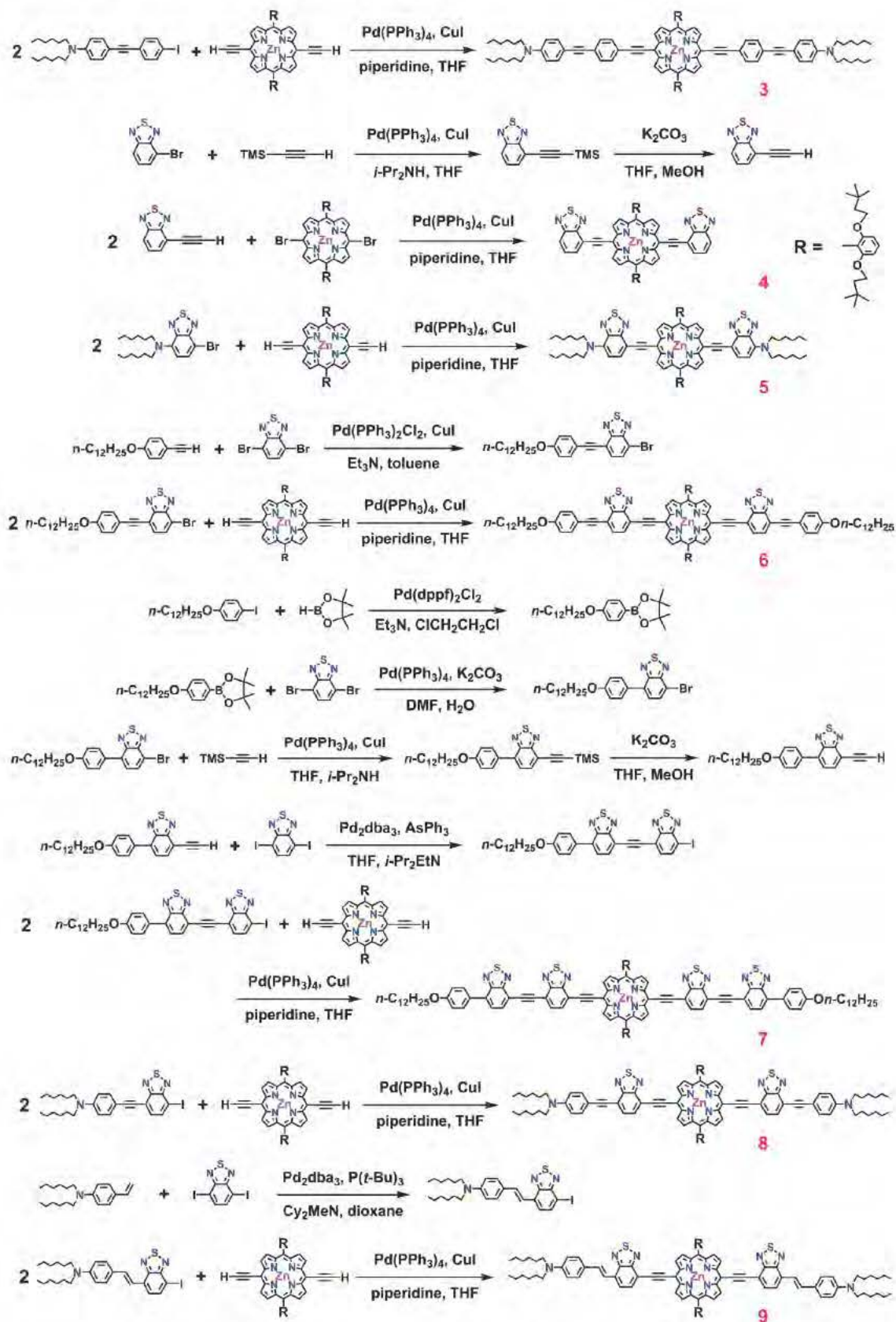
### Synthesis

Chromophores **2–9** are based on a (5,15-diethynylporphinato)zinc(II) framework and feature symmetric donor or acceptor units appended at the *meso*-ethynyl positions that derive from phenylene and benzo[c][1,2,5]thiadiazole building blocks; these structures, along with the TMS-protected (5,15-diethynyl-10,20-bis[3',5'-bis(9''-methoxy-1'',4'',7''-trioxanonyl)phenyl]porphinato)zinc(II) reference monomer (**1**), are shown in Fig. 1. Scheme 1 details the syntheses of fluorophores **3–9**. The proquinoidal spacer unit, benzo[c][1,2,5]thiadiazole, which extends  $\pi$ -conjugation from the porphyrin core for **4–9**, has been used not only as a common building block to enhance electronic delocalization within  $\pi$ -conjugated oligomers and polymers, but also as an electron accepting moiety [55, 99, 101, 102]. Incorporation of benzo[c][1,2,5]thiadiazole into conjugated organic networks is made

facile through the agency of palladium-catalyzed cross-coupling reactions. In **2–9**, each aromatic unit is linked by either ethyne or ethene units through Sonogashira or Heck coupling reactions. The 10- and 20-*meso*-positions of the (porphinato)zinc cores of **1–9** feature either 3,5-bis(9'-methoxy-1',4',7'-trioxanonyl)phenyl (**1**) or 2,6-bis(3',3'-dimethyl-1'-butyloxy)phenyl substituents (**2–9**) to ensure high solubility. Fluorophores **2–9** were synthesized by Pd-mediated cross-coupling reactions involving appropriately modified terminal substituents and 5,15-dibromo- or 5,15-diethynyl(porphinato)zinc(II) synthons (Experimental Section).

### Steady-state electronic absorption spectra

Electronic absorption spectra of NIR fluorophores **2–9** recorded in THF solvent are displayed in Fig. 2. These chromophores feature lowest energy Q absorption bands that are significantly red-shifted (1985–3070 cm<sup>−1</sup>) and intensified (~20 to 50-fold enhanced in oscillator strength) relative to the analogous transition manifold of [5,10,15,20-tetraphenyl(porphinato)]zinc(II) (**TPPZn**) [100]. While chromophores **2** and **3** manifest spectral signatures akin to other closely related, [5,15-bis[(aryl)ethynyl]-10,20-diphenylporphinato]zinc(II) complexes [42], note that structures **4–9**, which incorporate benzo[c][1,2,5]thiadiazole units, manifest spectra that bear distinct similarities to chlorophylls and structurally related molecules [103]. The extinction coefficients of the x-polarized Q-band [Q<sub>x</sub>(0,0)] transitions for **4–9** are significantly enhanced relative to **2** and **3**, which bear 5,15-bis(arylethynyl) macrocycle substituents (Fig. 2, Table 1). As conjugation is expanded at the porphyrin (5,15-bis(benzo[c][1',2',5']thiadiazol-4'-ylethynyl) moieties [4→5→(6, 7, 8, 9)] (Fig. 2, Table 1), increasingly pronounced B-state (Soret) transition manifold splitting is evident; note that the Q<sub>x</sub>(0,0) transition extinction coefficients for fluorophores **6–9** surpass those of their most intense respective B-band absorption, and exceed 10<sup>5</sup> M<sup>−1</sup>·cm<sup>−1</sup>, a value comparable to Q-state absorptions characteristic of chlorophylls and phthalocyanines [30, 37]. In contrast to the full widths at half maximum (FWHM) values for the B-band manifolds of **6–9**, which span 4430–6480 cm<sup>−1</sup> and greatly exceed that of the **TPPZn** benchmark (660 cm<sup>−1</sup>), the FWHMs of their respective Q<sub>x</sub>(0,0) transitions range from 812 to 940 cm<sup>−1</sup>. Compounds **3** and **8** highlight the qualitative impact of 5,15-bis(benzo[c][1',2',5']thiadiazol-4'-ylethynyl) substituents relative to corresponding 5,15-bis[(aryl)ethynyl] groups upon the (porphinato)zinc chromophore long-wavelength absorption maximum: note the x-polarized Q-state absorption maximum for **8** is 928 cm<sup>−1</sup> red-shifted relative to that for **3**. The enhanced  $\pi$ -conjugation afforded by the benzo[c][1,2,5]thiadiazolyl group is consistent with its proquinoidal character [104], and earlier work which establishes that *meso* (benzo[c][1,2,5]thiadiazol-4-ylethynyl) substituents



Scheme 1. Synthetic routes to 5,15-diethynyl-(porphinato)zinc(II)-based fluorophores 3–9 and to key precursor compounds

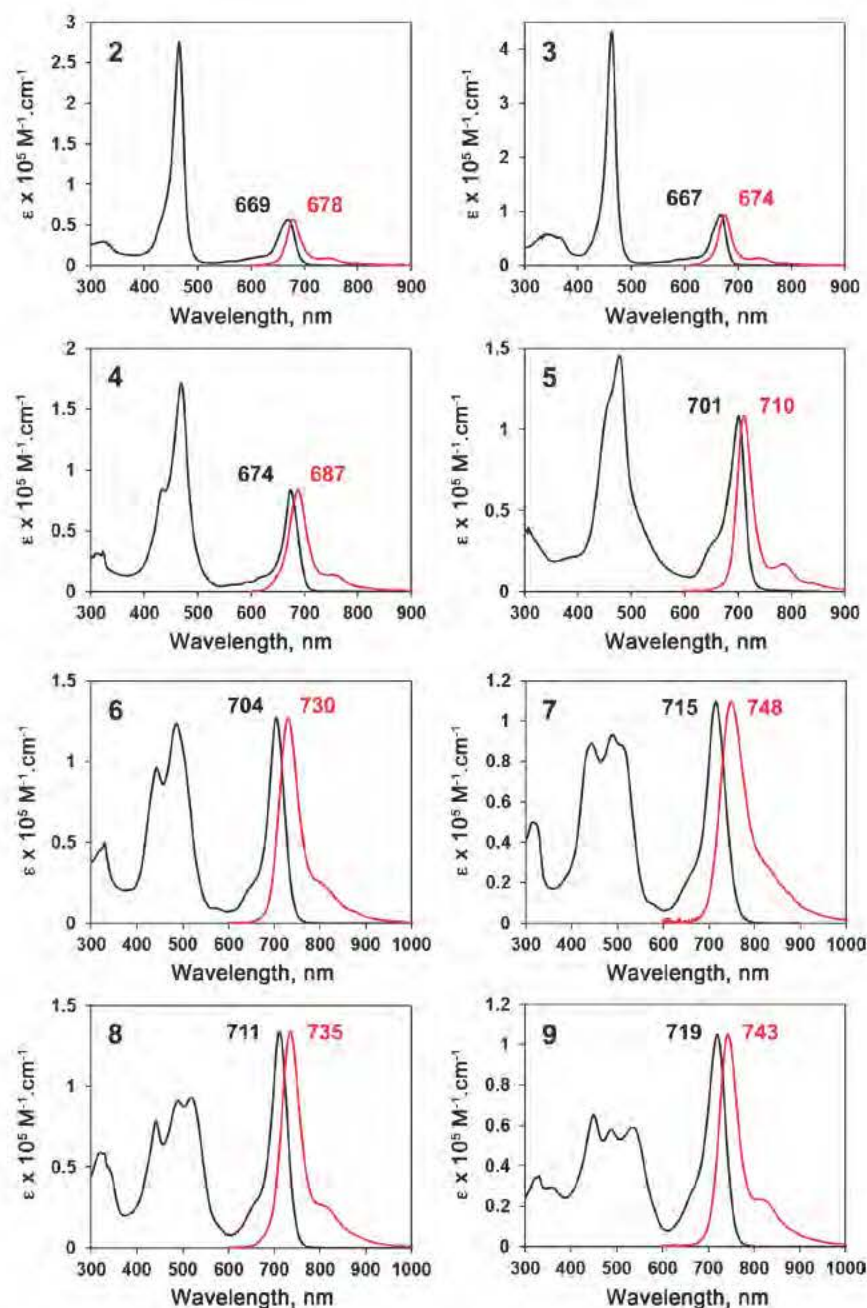


Fig. 2. Absorption (black line) and fluorescence (red line) spectra of 5,15-diethynyl-(porphinato)zinc(II)-based fluorophores 2–9 recorded in THF solvent

drive pronounced  $S_1$  state cumulenenic character for (porphinato)zinc-based chromophores [55].

### Fluorescence spectra

Figure 2 also highlights the fluorescence spectra recorded for chromophores 2–9 in THF solvent; these spectra mirror the respective lowest energy Q-state absorption manifolds for these chromophores. The fluorescence energy maxima red-shift with increasing

degrees of conjugation [4→5→(6, 7, 8, 9)] (Fig. 2, Table 1); note in this regard that fluorophore 7 features an emission band maximum centered at 748 nm, and that structures 2–9 feature narrow fluorescence bands ( $620\text{ cm}^{-1} < \text{FWHM}(S_1 \rightarrow S_0) < 1130\text{ cm}^{-1}$ ) that are significantly reduced with respect to the  $S_1 \rightarrow S_0$  FWHM value determined for TPPZn ( $1924\text{ cm}^{-1}$ ). Note also that the narrow fluorescence bands of 2–9 resemble the spectral breadths of their respective lowest energy Q-state absorption manifolds (Table 1) and feature low-magnitude

**Table 1.** Comparative electronic absorption and steady-state fluorescence spectral data determined for chromophores 1–9 in THF solvent relative to the **TPPZn** benchmark

	$\lambda_{\max}(S_0 \rightarrow S_1)$ , nm <sup>a</sup>	$\epsilon_{\max}(S_0 \rightarrow S_1)$ , M <sup>-1</sup> ·cm <sup>-1a</sup>	FWHM (S <sub>0</sub> →S <sub>1</sub> ), cm <sup>-1a</sup>	$\lambda_{\max}(S_1 \rightarrow S_0)$ , nm	FWHM (S <sub>1</sub> →S <sub>0</sub> ), cm <sup>-1</sup>	Stokes shift, cm <sup>-1c</sup>
<b>TPPZn</b> (in benzene)	589	3680	577	605	1924 <sup>b</sup>	449
<b>1</b>	632	33,200	438	638	626	149
<b>2</b>	669	57,000	824	678	656	198
<b>3</b>	667	94,000	704	674	618	156
<b>4</b>	674	84,000	654	687	809	281
<b>5</b>	701	108,000	737	710	649	181
<b>6</b>	704	127,000	812	730	922	506
<b>7</b>	715	109,400	939	748	1131	617
<b>8</b>	711	134,000	818	735	890	459
<b>9</b>	719	105,000	940	743	870	449

<sup>a</sup>For 1–9, the value reported corresponds to that for the x-polarized (S<sub>0</sub>→S<sub>1</sub>) absorption. Note that for the **TPPZn** chromophore, the value reported corresponds to that for the Q(0,0) transition. <sup>b</sup>The value reported corresponds to that for the Q-state manifold. <sup>c</sup>The difference in energy between the absorption (S<sub>0</sub>→S<sub>1</sub>) and fluorescence (S<sub>1</sub>→S<sub>0</sub>) band maxima.

**Table 2.** Comparative x-polarized [S<sub>0</sub>→S<sub>1</sub>; Q<sub>x</sub>(0,0)] integrated absorptive oscillator strengths, fluorescence quantum yields, fluorescence lifetimes, experimental and calculated radiative rate constants, and experimental non-radiative rate constants determined for chromophores 1–9 in THF solvent relative to the **TPPZn** benchmark

	Oscillator strength <sup>a</sup>	$\Phi_f^b$	$\tau_f$ , ns	$k_r$ (× 10 <sup>7</sup> s <sup>-1</sup> )	$k_{nr}$ (× 10 <sup>7</sup> s <sup>-1</sup> )	$k_r(\text{calc})^d$ (× 10 <sup>7</sup> s <sup>-1</sup> )
<b>TPPZn</b> (in benzene)	0.00977	0.033 <sup>c</sup>	2.09	1.58	46.27	1.78
<b>1</b>	0.0669	0.058 (0.021)	1.99	2.91	47.34	4.30
<b>2</b>	0.216	0.22 (0.044)	2.04	10.78	38.24	7.72
<b>3</b>	0.304	0.25 (0.043)	1.63	15.34	46.01	11.1
<b>4</b>	0.253	0.15 (0.013)	1.42	10.56	59.86	9.23
<b>5</b>	0.366	0.19 (0.012)	1.20	15.83	67.50	11.3
<b>6</b>	0.474	0.32 (0.020)	1.97	16.24	34.52	13.0
<b>7</b>	0.473	0.35 (0.035)	1.87	18.72	34.76	11.8
<b>8</b>	0.504	0.36 (0.032)	1.71	21.05	37.43	13.8
<b>9</b>	0.454	0.26 (0.029)	1.37	18.98	54.01	11.5

<sup>a</sup> $f = 4.6 \times 10^{-9} \cdot \epsilon_{\max} \cdot \Delta\nu_{1/2}$ ; the oscillator strengths were calculated for the x-polarized (S<sub>0</sub>→S<sub>1</sub>) absorption. Note that for the **TPPZn** chromophore, the reported integrated oscillator strength corresponds to that for the Q-state transition manifold. <sup>b</sup>Fluorescence quantum yields determined relative to free base TPP in benzene ( $\Phi_f = 0.13$ ); parenthetical values represent standard deviations from the mean. <sup>c</sup>From Ref. 100. <sup>d</sup>Calculated using Equation 2.

Stokes shifts (155–620 cm<sup>-1</sup>), congruent with a minimal degree of excited-state structural relaxation relative the ground-state conformation for these chromophores.

#### Strickler–Berg analysis of the S<sub>1</sub>-state photophysics of fluorophores 2–9

Relative to the (porphinato)zinc chromophore **TPPZn** ( $\Phi_f = 0.033$ ), the fluorescence quantum yields of fluorophores 2–9 are particularly dramatic (0.15 <

$\Phi_f < 0.36$ ; Table 2). Further, given the shape and intensity of the steady-state fluorescence spectra of these monomeric (porphinato)zinc chromophores that bear either 5,15-bis[(aryl)ethynyl] or 5,15-bis(benzo[c][1',2',5']thiadiazol-4'-ylethynyl) substituents, coupled with the fact that the emission band maxima of these species are significantly red-shifted (1690–3160 cm<sup>-1</sup>) with respect to the **TPPZn** benchmark (Table 1), suggest an analysis of the S<sub>1</sub> state photophysics within the context of the Strickler–Berg model, which relates increases in

the integrated oscillator strength of the lowest-energy ground-state absorption band with a corresponding augmentation of the radiative decay rate constant ( $k_r$ , Equation 2) [22].

$$k_r = 2.880 \times 10^{-9} n^2 \langle \tilde{\nu}_f^3 \rangle_{Av}^{-1} \frac{g_l}{g_u} \int \epsilon d \ln \tilde{\nu} \quad (2)$$

Here  $k_r$  is radiative decay rate constant,  $n$  is the refractive index of the solvent,  $g_l$  and  $g_u$  are the respective degeneracies of the ground and excited states,  $\epsilon$  is the molar extinction coefficient,  $\nu$  is the frequency of the transition in  $\text{cm}^{-1}$ . The term  $\langle \tilde{\nu}_f^3 \rangle_{Av}^{-1}$  is expressed as:

$$\langle \tilde{\nu}_f^3 \rangle_{Av}^{-1} = \frac{\int I(\nu) d\nu}{\int \nu^3 I(\nu) d\nu} \quad (3)$$

where  $I$  is the intensity of the fluorescence spectrum, measured in terms of relative numbers of quanta at each frequency. The fluorescence quantum yield ( $\Phi_f$ ) is simply described by Equation 4;

$$\Phi_f = \frac{k_r}{k_r + k_{nr}} \quad (4)$$

where  $k_{nr}$  describes the magnitude of the non-radiative decay rate constant, which corresponds to the sum of the internal conversion ( $k_{ic}$ ) and intersystem crossing ( $k_{isc}$ ) rate constants. Provided that the magnitudes of the non-radiative rate remain approximately constant within a family of closely related chromophores, an increase in the integrated oscillator strength results in a corresponding increase in the fluorescence quantum yield.

Figure 3 highlights the x-polarized Q-state oscillator strength dependent fluorescence quantum yields, radiative

rate constants, and non-radiative rate constants of fluorophores 1–9 relative to the TPPZn benchmark. Note the distinct increase in the magnitude of the radiative rate constant with increasing x-polarized Q-state oscillator strength (Fig. 3B), and that the measured  $k_r$  values for fluorophores 5–9 exceed that of the TPPZn by more than an order of magnitude. This apparent Stricker–Berg dependence of the radiative rate constant upon the integrated lowest energy  $S_0 \rightarrow S_1$  oscillator strength gives rise to a family of porphyrin-based NIR fluorophores in which the longest wavelength emitter (7, 748 nm) features a fluorescence quantum yield ( $\Phi_f = 0.35$ ; Tables 1 and 2) that exceeds that of chromophores 1–6 and 9, which emit to the blue of this wavelength.

As emission wavelengths approach the NIR spectral domain, the simple Stricker–Berg predicted dependence of the radiative rate constant upon the magnitude of the integrated oscillator strength is generally mitigated by expected energy gap law effects [23], where increasing magnitudes of the  $S_0 \rightarrow S_1$  internal conversion rate constant ( $k_{ic}$ ) track with diminishing  $S_0 \rightarrow S_1$  energy gaps and thus sharply decrease  $\Phi_f$ . In these chromophores, two factors conspire to enhance  $\Phi_f$  as emission wavelength increases over the 650–750 nm spectral domain. The first of these derives from the fact that the proquinoidal benzo[c][1,2,5]thiadiazole unit minimizes the extent of excited-state structural relaxation relative the ground-state conformation [55] for chromophores 4–9, reflected by the narrow fluorescence bands and modest Stokes shifts determined for these species (Fig. 2; Tables 1 and 2), and thereby reduces  $S_1 \rightarrow S_0$  Franck–Condon overlap important for determining the magnitude of  $k_{ic}$ . The second factor that drives this unusual dependence of  $\Phi_f$  upon emission wavelength stems from the fact that for these ethyne-laborated (porphinato)zinc derivatives, intersystem

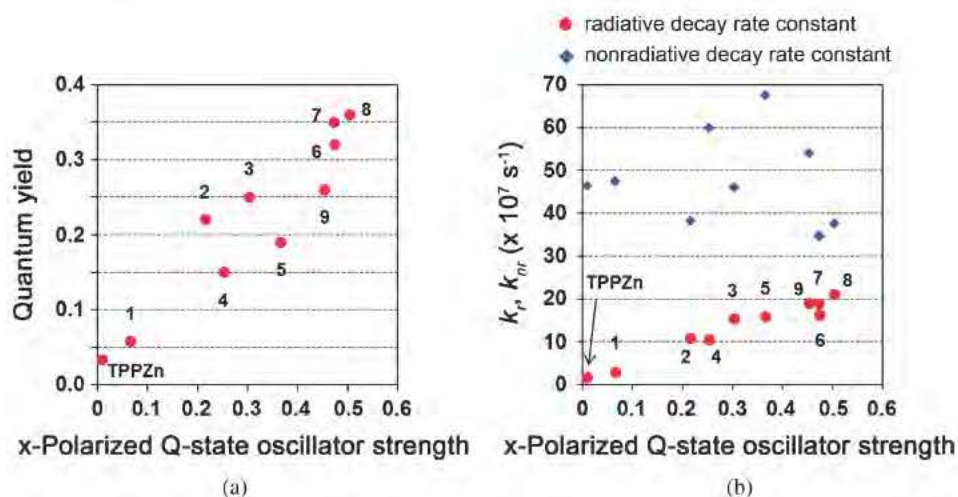


Fig. 3. x-Polarized Q-state [ $Q_x (S_0 \rightarrow S_1)$ ] oscillator strength dependent fluorescence quantum yields, radiative rate constants ( $k_r$ ), and non-radiative rate constants ( $k_{nr}$ ) of diethynyl(porphinato)zinc(II) derivatives (1–9) relative to the [5,10,15,20-tetraphenyl-(porphinato)]zinc(II) (TPPZn) benchmark. (a) x-Polarized Q-state oscillator strength dependence of the fluorescence quantum yield. (b) x-Polarized Q-state oscillator strength dependence of the radiative and non-radiative decay rate constant magnitudes

crossing into the triplet manifold generates  $T_1$  states that manifest more spatially confined excitations relative to the globally delocalized  $S_1$  states of these chromophores [41, 45, 47, 54, 62]. This diminished overlap of  $S_1$  and  $T_1$  state wavefunctions mitigates  $S_1$ - $T_1$  intersystem crossing rate constants ( $k_{isc}$  values), and thus serves to counter-balance the effect of augmented Franck–Condon mediated internal conversion that typically accompanies  $S_0$ - $S_1$  energy gap reductions; this effect has been detailed previously for closely related compounds [57]. Thus, for 4–9, extension of x-polarized conjugation of the (5,15-diethynylporphinato)zinc(II) framework *via* the benzo[c][1,2,5]thiadiazole moiety causes the magnitude of  $k_r$  to increase faster than does the magnitude of  $k_{nr}$  as emission wavelength increases, providing substantial fluorescence quantum yields that manifest a weak energy gap law [23] dependence over this spectral regime.

## CONCLUSION

We describe a design strategy for (porphinato)zinc-based chromophores that possess large NIR fluorescence quantum yields. These fluorophores are based on a (5,15-diethynylporphinato)zinc(II) framework and feature symmetric donor or acceptor units appended at the *meso*-ethynyl positions *via* benzo[c][1,2,5]thiadiazole moieties. These chromophores possess red-shifted absorption and emission bands relative to TPPZn and (5,15-diethynyl-10,20-arylporphinato)zinc(II) benchmarks that range between 650 and 750 nm and bear distinct spectral similarities to those manifest by chlorophylls and structurally related molecules.

Interestingly, the measured radiative decay rate constants for these emitters track with the integrated oscillator strengths of their respective x-polarized Q-band absorptions, and thus define an unusual family of high quantum yield NIR fluorophores in which emission intensity is governed by a simple Strickler–Berg dependence. These photophysical properties derive from the facts that: (i) the proquinoidal benzo[c][1,2,5]thiadiazole unit minimizes the extent of excited-state structural relaxation relative the ground-state conformation [55], and (ii) *meso*-ethynyl elaborated (porphinato)zinc compounds are characterized by  $T_1$  states that are more spatially confined than their globally delocalized  $S_1$  states [41, 45, 47, 54, 62], which result in diminished  $S_1$ - $T_1$  intersystem crossing rate constants relative to conventional (porphinato)zinc chromophores. For these NIR fluorophores, these effects cause the magnitude of  $k_r$  to increase faster than does the magnitude of  $k_{nr}$  as emission wavelength increases, providing substantial fluorescence quantum yields that manifest a weak energy gap law [23] dependence over the spectral regime (685–750 nm) spanned by these emitters. These designs that take advantage of these photophysical properties make possible broadly absorptive and strongly

emissive NIR fluorophores that derive from a monomeric (5,15-diethynyl-porphinato)zinc framework.

## Acknowledgements

This work was supported through the Department of Defense (W81XWH-13-1-0086). The authors thank Professor Felix N. Castellano and Dr. Radiy Islangulov for their assistance with fluorescence lifetime measurements.

## REFERENCES

1. Weissleder R. *Nat. Biotechnol.* 2001; **19**: 316–317.
2. Weissleder R and Ntziachristos V. *Nat. Med.* 2003; **9**: 123–128.
3. Bremer C, Ntziachristos V and Weissleder R. *Eur. Radiol.* 2003; **13**: 231–243.
4. Frangioni JV. *Curr. Opin. Chem. Biol.* 2003; **7**: 626–634.
5. Hilderbrand SA and Weissleder R. *Curr. Opin. Chem. Biol.* 2010; **14**: 71–79.
6. Martínez-Díaz MV, de la Torre G and Torres T. *Chem. Commun.* 2010; **46**: 7090–7108.
7. Liu Y, Lin H, Dy JT, Tamaki K, Nakazaki J, Nakayama D, Uchida S, Kubo T and Segawa H. *Chem. Commun.* 2011; **47**: 4010–4012.
8. Chang Y-C, Wang C-L, Pan T-Y, Hong S-H, Lan C-M, Kuo H-H, Lo C-F, Hsu H-Y, Lin C-Y and Diao EW-G. *Chem. Commun.* 2011; **47**: 8910–8912.
9. Mathew S, Yella A, Gao P, Humphry-Baker R, Curchod BFE, Ashari-Astani N, Tavernelli I, Rothlisberger U, Nazeeruddin MK and Grätzel M. *Nature Chem.* 2014; **6**: 242–247.
10. D'Souza F, Amin AN, El-Khouly ME, Subbaiyan NK, Zandler ME and Fukuzumi S. *J. Am. Chem. Soc.* 2012; **134**: 654–664.
11. Balzani V, Credi A and Venturi M. *ChemSusChem* 2008; **1**: 26–58.
12. Roncali J. *Chem. Rev.* 1997; **97**: 173–205.
13. van Mullekom HAM, Vekemans JAJM, Havinga EE and Meijer EW. *Mater. Sci. Eng.* 2001; **32**: 1–40.
14. Tsuda A and Osuka A. *Science* 2001; **293**: 79–82.
15. Kiyose K, Kojima H and Nagano T. *Chem. Asian J.* 2008; **3**: 506–515.
16. Escobedo JO, Rusin O, Lim S and Strongin RM. *Curr. Opin. Chem. Biol.* 2010; **14**: 64–70.
17. Qian G and Wang ZY. *Chem. Asian J.* 2010; **5**: 1006–1029.
18. Luo S, Zhang E, Su Y, Cheng T and Shi C. *Biomaterials* 2011; **32**: 7127–7138.
19. Mori H, Tanaka T and Osuka A. *J. Mater. Chem. C* 2013; **1**: 2500–2519.
20. Zhao W and Carreira EM. *Angew. Chem. Int. Ed.* 2005; **44**: 1677–1679.
21. Umezawa K, Nakamura Y, Makino H, Citterio D and Suzuki K. *J. Am. Chem. Soc.* 2008; **130**: 1550–1551.

22. Strickler SJ and Berg RA. *J. Chem. Phys.* 1962; **37**: 814–822.
23. Englman R and Jortner J. *Mol. Phys.* 1970; **18**: 145–164.
24. Gouterman M. *J. Mol. Spectrosc.* 1961; **6**: 138–163.
25. Finikova OS, Cheprakov AV and Vinogradov SA. *J. Org. Chem.* 2005; **70**: 9562–9572.
26. Nakamura J, Okujima T, Tomimori Y, Komobuchi N, Yamada H, Uno H and Ono N. *Heterocycles* 2010; **80**: 1165–1175.
27. Davis NKS, Thompson AL and Anderson HL. *Org. Lett.* 2010; **12**: 2124–2127.
28. Davis NKS, Thompson AL and Anderson HL. *J. Am. Chem. Soc.* 2011; **133**: 30–31.
29. Diev VV, Schlenker CW, Hanson K, Zhong Q, Zimmerman JD, Forrest SR and Thompson ME. *J. Org. Chem.* 2012; **77**: 143–159.
30. Sauer K, Smith JRL and Schultz AJ. *J. Am. Chem. Soc.* 1966; **88**: 2681–2688.
31. Connolly JS, Samuel EB and Janzen AF. *Photochem. Photobiol.* 1982; **36**: 565–574.
32. Forster LS and Livingston R. *J. Chem. Phys.* 1952; **20**: 1315–1320.
33. Kee HL, Kirmaier C, Tang Q, Diers JR, Muthiah C, Taniguchi M, Laha JK, Ptaszek M, Lindsey JS, Bocian DF and Holtz D. *Photochem. Photobiol.* 2007; **83**: 1110–1124.
34. Taniguchi M, Cramer DL, Bhise AD, Kee HL, Bocian DF, Holtz D and Lindsey JS. *New J. Chem.* 2008; **32**: 947–958.
35. Kozyrev A, Ethirajan M, Chen P, Ohkubo K, Robinson BC, Barkigia KM, Fukuzumi S, Kadish KM and Pandey RK. *J. Org. Chem.* 2012; **77**: 10260–10271.
36. Seybold PG and Gouterman M. *J. Mol. Spectrosc.* 1969; **31**: 1–13.
37. Kobayashi N, Ogata H, Nonaka N and Luk'yanets EA. *Chem. Eur. J.* 2003; **9**: 5123–5134.
38. Susumu K, Maruyama H, Kobayashi H and Tanaka K. *J. Mater. Chem.* 2001; **11**: 2262–2270.
39. Lin VS-Y, DiMaggio SG and Therien MJ. *Science* 1994; **264**: 1105–1111.
40. Lin VS-Y and Therien MJ. *Chem. Eur. J.* 1995; **1**: 645–651.
41. Angiolillo PJ, Lin VS-Y, Vanderkooi JM and Therien MJ. *J. Am. Chem. Soc.* 1995; **117**: 12514–12527.
42. LeCours SM, DiMaggio SG and Therien MJ. *J. Am. Chem. Soc.* 1996; **118**: 11854–11864.
43. LeCours SM, Philips CM, de Paula JC and Therien MJ. *J. Am. Chem. Soc.* 1997; **119**: 12578–12589.
44. Kumble R, Palese S, Lin VS-Y, Therien MJ and Hochstrasser RM. *J. Am. Chem. Soc.* 1998; **120**: 11489–11498.
45. Shediak R, Gray MHB, Uyeda HT, Johnson RC, Hupp JT, Angiolillo PJ and Therien MJ. *J. Am. Chem. Soc.* 2000; **122**: 7017–7033.
46. Fletcher JT and Therien MJ. *J. Am. Chem. Soc.* 2000; **122**: 12393–12394.
47. Angiolillo PJ, Susumu K, Uyeda HT, Lin VS-Y, Shediak R and Therien MJ. *Synth. Met.* 2001; **116**: 247–253.
48. Fletcher JT and Therien MJ. *Inorg. Chem.* 2002; **41**: 331–341.
49. Fletcher JT and Therien MJ. *J. Am. Chem. Soc.* 2002; **124**: 4298–4311.
50. Susumu K and Therien MJ. *J. Am. Chem. Soc.* 2002; **124**: 8550–8552.
51. Rubtsov IV, Susumu K, Rubtsov GI and Therien MJ. *J. Am. Chem. Soc.* 2003; **125**: 2687–2696.
52. Redmore NP, Rubtsov IV and Therien MJ. *J. Am. Chem. Soc.* 2003; **125**: 8769–8778.
53. Rubtsov IV, Redmore NP, Hochstrasser RM and Therien MJ. *J. Am. Chem. Soc.* 2004; **126**: 2684–2685.
54. Angiolillo PJ, Uyeda HT, Duncan TV and Therien MJ. *J. Phys. Chem. B* 2004; **108**: 11893–11903.
55. Susumu K, Duncan TV and Therien MJ. *J. Am. Chem. Soc.* 2005; **127**: 5186–5195.
56. Susumu K, Frail PR, Angiolillo PJ and Therien MJ. *J. Am. Chem. Soc.* 2006; **128**: 8380–8381.
57. Duncan TV, Susumu K, Sinks LE and Therien MJ. *J. Am. Chem. Soc.* 2006; **128**: 9000–9001.
58. Duncan TV, Wu SP and Therien MJ. *J. Am. Chem. Soc.* 2006; **128**: 10423–10435.
59. Frail PR, Susumu K, Huynh M, Fong J, Kikkawa JM and Therien MJ. *Chem. Mater.* 2007; **19**: 6062–6064.
60. Duncan TV, Ishizuka T and Therien MJ. *J. Am. Chem. Soc.* 2007; **129**: 9691–9703.
61. Duncan TV, Frail PR, Miloradovic IR and Therien MJ. *J. Phys. Chem. B* 2010; **114**: 14696–14702.
62. Angiolillo PJ, Rawson J, Frail PR and Therien MJ. *Chem. Commun.* 2013; **49**: 9722–9724.
63. LeCours SM, Guan H-W, DiMaggio SG, Wang CH and Therien MJ. *J. Am. Chem. Soc.* 1996; **118**: 1497–1503.
64. Priyadarshy S, Therien MJ and Beratan DN. *J. Am. Chem. Soc.* 1996; **118**: 1504–1510.
65. Karki L, Vance FW, Hupp JT, LeCours SM and Therien MJ. *J. Am. Chem. Soc.* 1998; **120**: 2606–2611.
66. Uyeda HT, Zhao Y, Wostyn K, Asselberghs I, Clays K, Persoons A and Therien MJ. *J. Am. Chem. Soc.* 2002; **124**: 13806–13813.
67. Duncan TV, Rubtsov IV, Uyeda HT and Therien MJ. *J. Am. Chem. Soc.* 2004; **126**: 9474–9475.
68. Zhang T-G, Zhao Y, Asselberghs I, Persoons A, Clays K and Therien MJ. *J. Am. Chem. Soc.* 2005; **127**: 9710–9720.
69. Zhang T-G, Zhao Y, Song K, Asselberghs I, Persoons A, Clays K and Therien MJ. *Inorg. Chem.* 2006; **45**: 9703–9712.
70. Xu T, Wu SP, Miloradovic I, Therien MJ and Blasie JK. *Nano Lett.* 2006; **6**: 2387–2394.
71. Duncan TV, Song K, Hung S-T, Miloradovic I, Nayak A, Persoons A, Verbiest T, Therien MJ and Clays K. *Angew. Chem. Int. Ed.* 2008; **47**: 2978–2981.

72. Keinan S, Therien MJ, Beratan DN and Yang W. *J. Phys. Chem. A* 2008; **112**: 12203–12207.
73. Therien MJ. *Nature* 2009; **458**: 716–717.
74. Hu X, Xiao D, Keinan S, Asselberghs I, Therien MJ, Clays K, Yang W and Beratan DN. *J. Phys. Chem. C* 2010; **114**: 2349–2359.
75. Gonella G, Dai H-L, Fry HC, Therien MJ, Krishnan V, Tronin A and Blasie JK. *J. Am. Chem. Soc.* 2010; **132**: 9693–9700.
76. Krishnan V, Tronin A, Strzalka J, Fry HC, Therien MJ and Blasie JK. *J. Am. Chem. Soc.* 2010; **132**: 11083–11092.
77. Singh-Rachford TN, Nayak A, Muro-Small ML, Goeb S, Therien MJ and Castellano FN. *J. Am. Chem. Soc.* 2010; **132**: 14203–14211.
78. Ishizuka T, Sinks LE, Song K, Hung S-T, Nayak A, Clays K and Therien MJ. *J. Am. Chem. Soc.* 2011; **133**: 2884–2896.
79. Jiang N, Zuber G, Keinan S, Nayak A, Yang W, Therien MJ and Beratan DN. *J. Phys. Chem. C* 2012; **116**: 9724–9733.
80. Fry HC, Lehmann A, Sinks LE, Asselberghs I, Tronin A, Krishnan V, Blasie JK, Clays K, DeGrado WF, Saven JG and Therien MJ. *J. Am. Chem. Soc.* 2013; **135**: 13914–13926.
81. Deria P, Bargaen CDV, Olivier J-H, Kumbhar AS, Saven JG and Therien MJ. *J. Am. Chem. Soc.* 2013; **135**: 16220–16234.
82. Ostrowski JC, Susumu K, Robinson MR, Therien MJ and Bazan GC. *Adv. Mater.* 2003; **15**: 1296–1300.
83. Banerjee P, Conklin D, Nanayakkara S, Park T-H, Therien MJ and Bonnell DA. *ACS Nano* 2010; **4**: 1019–1025.
84. Conklin D, Park T-H, Nanayakkara S, Therien MJ and Bonnell DA. *Adv. Funct. Mater.* 2011; **21**: 4712–4718.
85. Conklin D, Nanayakkara S, Park T-H, Lagadec MF, Stecher JT, Therien MJ and Bonnell DA. *Nano Lett.* 2012; **12**: 2414–2419.
86. Li Z, Park T-H, Rawson J, Therien MJ and Borguet E. *Nano Lett.* 2012; **12**: 2722–2727.
87. Conklin D, Nanayakkara S, Park T-H, Lagadec MF, Stecher JT, Chen X, Therien MJ and Bonnell DA. *ACS Nano* 2013; **7**: 4479–4486.
88. Ghoroghchian PP, Frail PR, Susumu K, Blessington D, Brannan AK, Bates FS, Chance B, Hammer DA and Therien MJ. *Proc. Natl. Acad. Sci. USA* 2005; **102**: 2922–2927.
89. Ghoroghchian PP, Frail PR, Susumu K, Park T-H, Wu SP, Uyeda HT, Hammer DA and Therien MJ. *J. Am. Chem. Soc.* 2005; **127**: 15388–15390.
90. Wu SP, Lee I, Ghoroghchian PP, Frail PR, Zheng G, Glickson JD and Therien MJ. *Bioconjugate Chem.* 2005; **16**: 542–550.
91. Ghoroghchian PP, Lin JJ, Brannan AK, Frail PR, Bates FS, Therien MJ and Hammer DA. *Soft Matter* 2006; **2**: 973–980.
92. Ghoroghchian PP, Frail PR, Li G, Zupancich JA, Bates FS, Hammer DA and Therien MJ. *Chem. Mater.* 2007; **19**: 1309–1318.
93. Christian NA, Milone MC, Ranka SS, Li G, Frail PR, Davis KP, Bates FS, Therien MJ, Ghoroghchian PP, June CH and Hammer DA. *Bioconjugate Chem.* 2007; **18**: 31–40.
94. Duncan TV, Ghoroghchian PP, Rubtsov IV, Hammer DA and Therien MJ. *J. Am. Chem. Soc.* 2008; **130**: 9773–9784.
95. Ghoroghchian PP, Therien MJ and Hammer DA. *Wiley Interdiscip. Rev.: Nanomed. Nanobiotechnol.* 2009; **1**: 156–167.
96. Christian NA, Benencia F, Milone MC, Li G, Frail PR, Therien MJ, Coukos G and Hammer DA. *Mol. Imaging Biol.* 2009; **11**: 167–177.
97. Kamat NP, Liao Z, Moses LE, Rawson J, Therien MJ, Dmochowski IJ and Hammer DA. *Proc. Natl. Acad. Sci. U.S.A.* 2011; **108**: 13984–13989.
98. Pilgram K, Zupan M and Skiles R. *J. Heterocycl. Chem.* 1970; **7**: 629–633.
99. Susumu K, Fisher JAN, Zheng J, Beratan DN, Yodh AG and Therien MJ. *J. Phys. Chem. A* 2011; **115**: 5525–5539.
100. Quimby DJ and Longo FR. *J. Am. Chem. Soc.* 1975; **97**: 5111–5117.
101. Velusamy M, Justin Thomas KR, Lin JT, Hsu Y-C and Ho K-C. *Org. Lett.* 2005; **7**: 1899–1902.
102. Bundgaard E and Krebs FC. *Sol. Energy Mater. Sol. Cells* 2007; **91**: 954–985.
103. Linnanto J and Korppi-Tommola J. *J. Phys. Chem. A* 2001; **105**: 3855–3866.
104. Neto BAD, Lapis AAM, Júnior ENdS and Dupont J. *Eur. J. Org. Chem.* 2013: 228–255.

---

## BIOGRAPHICAL SKETCH

---

NAME	POSITION TITLE
Michael J. Therien	William R. Kenan, Jr. Professor

EDUCATION/TRAINING			
INSTITUTION AND LOCATION	DEGREE	YEAR(s)	FIELD OF STUDY
University of California, Los Angeles, CA	B. S.	1982	Chemistry
University of California, San Diego, CA	Ph.D.	1987	Chemistry
California Institute of Technology, Pasadena, CA	NIH PostDoc	1987-1990	Chemistry

### RESEARCH AND PROFESSIONAL EXPERIENCE:

#### Positions Held:

University of Pennsylvania	Assistant Professor	1990-1996
University of Pennsylvania	Associate Professor	1996-1997
University of Pennsylvania	Professor of Chemistry	1997-2002
Princeton University	Visiting Professor	2002
University of Pennsylvania	Alan G. MacDiarmid Professor of Chemistry	2002-2007
Universiteit of Lueven	Visiting Professor	2004; 2005
Universiteit of Leuven	Francqui International Professor	2008-2009
Duke University	Professor of Chemistry	2008
Duke University	William R. Kenan, Jr. Professor	2009-present
University of Bordeaux	Visiting Professor	2010

#### Honors:

National Institutes of Health Postdoctoral Research Fellow (1987-1990); Searle Scholar (1991-1994); Arnold and Mabel Beckman Foundation Young Investigator (1992-1994); National Science Foundation Young Investigator (1993-1998); E. I. DuPont de Nemours Young Faculty Award (1995-1997); Alfred P. Sloan Foundation Fellow (1995-1997); Camille Dreyfus Teacher-Scholar (1997-2002); Journal of Porphyrins and Phthalocyanines Young Investigator Award (2002); Pederson Lecturer, Central Research and Development Division, E. I. DuPont de Nemours (2003); American Chemical Society Philadelphia Section Award (2004); W. Heinlen Hall Lectureship, Bowling Green State University (2005); Elected Fellow, American Association for the Advancement of Science (2005); International Francqui Chair, Belgium (2008-2009); Fellow, Flemish Academy of Science (2009).

#### Advisory Positions:

External Reviewer, United States Department of Energy, Nanotechnology Centers (2003-2009); Review Committee Member, Beckman Young Investigator Program (2003-present); Research Team Leader, NSF-supported Nanoscience and Technology Center (2004-2008); Scientific Advisory Board, Center for Nanoscale Materials, Argonne National Laboratory (2005-2014); ARPA-E Photovoltaics Review Committee Chair (2009); External Program Reviewer, Scientific Foundation Ireland (2011); Molecular Assemblies Research Team Leader, DOE Energy Frontier Research Center for Solar Fuels (2012-2014).

#### Earlier Publications Pertinent to this Application:

- 1) Highly-Conjugated, Acetylenyl-Bridged Porphyrins: New Models for Light-Harvesting Antenna Systems, V. S.-Y. Lin, S. G. DiMaggio, and M. J. Therien, *Science (Washington, D. C.)* **1994**, 264, 1105-1111.

- 2) The Role of Porphyrin-to-Porphyrin Linkage Topology in the Extensive Modulation of the Absorptive and Emissive Properties of a Series of Ethynyl- and Butadiynyl-Bridged Bis- and Tris(porphinato)zinc Chromophores, V. S.-Y. Lin and M. J. Therien, *Chem. Eur. J.* **1995**, *1*, 645-651.
- 3) Ultrafast Dynamics of Highly Conjugated Porphyrin Arrays, R. Kumble, S. Palese, V. S.-Y. Lin, M. J. Therien, and R. M. Hochstrasser, *J. Am. Chem. Soc.* **1998**, *120*, 11489-11498.
- 4) NIR-Emissive Polymersomes: Self-assembled Soft Matter for *in vivo* Optical Imaging, P. P. Ghoroghchian, P. R. Frail, K. Susumu, D. Blessington, A. K. Brannan, F. S. Bates, B. Chance, D. A. Hammer, and M. J. Therien, *Proc. Natl. Acad. Sci. U.S.A.* **2005**, *102*, 2922-2927.
- 5) Near-Infrared Optical Imaging of B16 Melanoma Cells via Low-Density Lipoprotein-Mediated Uptake and Delivery of High Emission Dipole Strength Tris[(Porphinato)Zinc(II)] Fluorophores, S. P. Wu, I. Lee, P. P. Ghoroghchian, P. R. Frail, G. Zheng, J. D. Glickson, and M. J. Therien, *Bioconjugate Chem.* **2005**, *16*, 542-550.
- 6) Broad Spectral Domain Fluorescence Wavelength Modulation of Visible and Near Infrared-Emissive Polymersomes, P. P. Ghoroghchian, P. R. Frail, K. Susumu, T.-H. Park, S. P. Wu, H. T. Uyeda, D. A. Hammer, and M. J. Therien, *J. Am. Chem. Soc.* **2005**, *127*, 15388-15390.
- 7) Bioresorbable Vesicles Formed through Spontaneous Self-Assembly of Amphiphilic Polyethyleneoxide-Block-Polycaprolactone, P. P. Ghoroghchian, G. Li, D. H. Levine, K. P. Davis, F. S. Bates, D. A. Hammer, and M. J. Therien, *Macromolecules* **2006**, *39*, 1673-1675.
- 8) Exceptional Near Infrared Fluorescence Quantum Yields and Excited-State Absorptivity of Conjugated Porphyrin Arrays, T. V. Duncan, K. Susumu, L. E. Sinks, and M. J. Therien, *J. Am. Chem. Soc.* **2006**, *128*, 9000-9001.
- 9) Quantitative Loading, Steady-State Emission, and Mechanical Stability of Near Infrared Emissive Polymersomes, P. P. Ghoroghchian, J. J. Lin, A. K. Brannan, P. R. Frail, F. S. Bates, M. J. Therien, and D. A. Hammer, *Soft Matter* **2006**, *2*, 973-980.
- 10) Tat-Functionalized Near-Infrared Polymersomes for Dendritic Cell Labeling, N. A. Christian, M. C. Milone, S. S. Ranka, G. Li, P. R. Frail, K. P. Davis, F. S. Bates, M. J. Therien, P. P. Ghoroghchian, C. H. June, and D. A. Hammer, *Bioconjugate Chem.* **2007**, *18*, 31-40.
- 11) Controlling Bulk Optical Properties of Emissive Polymersomes Through Intramembranous Polymer-Fluorophore Interactions, P. P. Ghoroghchian, P. R. Frail, G. Li, J. A. Zupancich, F. S. Bates, D. A. Hammer, and M. J. Therien, *Chem. Mater.* **2007**, *19*, 1309-1318.
- 12) Ultrafast Excited State Dynamics of Nanoscale Near Infrared Emissive Polymersomes, T. V. Duncan, P. P. Ghoroghchian, I. V. Rubstov, D. A. Hammer, and M. J. Therien, *J. Am. Chem. Soc.* **2008**, *130*, 9773-9784.
- 13) Using  $\alpha$ -Helical Coiled-Coils to Design Nanostructured Porphyrin Arrays, K. A. McAllister, H. Zou, F. V. Cochran, G. M. Bender, A. Senes, H. C. Fry, V. Nanda, P. A. Keenan, J. D. Lear, M. J. Therien, J. K. Blasie, and W. F. DeGrado, *J. Am. Chem. Soc.* **2008**, *130*, 11921-11927.
- 14) Leuko-Polymersomes, D. A. Hammer, G. R. Robbins, J. J. Lin, L. A. Smith, P. P. Ghoroghchian, M. J. Therien, and F. S. Bates, *Faraday Discuss.* **2008**, *139*, 129-141.
- 15) Polymersomes: A New Multi-Functional Tool for Cancer Diagnosis and Therapy, D. H. Levine, P. P. Ghoroghchian, J. Freudenberg, G. Zhang, M. J. Therien, M. I. Greene, D. A. Hammer, and R. Murali, *Methods* **2008**, *46*, 25-32.
- 16) In Vivo Fluorescence Imaging: A Personal Perspective, P. P. Ghoroghchian, M. J. Therien, and D. A. Hammer, *Wiley Interdisciplinary Reviews: Nanomedicine and Nanobiotechnology*, **2009**, *1*, 156-167.
- 17) Photo-initiated Destruction of Composite Porphyrin-Protein Polymersomes, M. Jimbo, G. P. Robbins, J. Swift, M. J. Therien, D. A. Hammer, and I. J. Dmochowski, *J. Am. Chem. Soc.* **2009**, *131*, 3872-3874.
- 18) In Vivo Dendritic Cell Tracking Using Fluorescence Lifetime Imaging and Near-Infrared Emissive Polymersomes, N. A. Christian, F. Benencia, M. C. Milone, G. Li, P. R. Frail, M. J. Therien, G. Coukos, and D. A. Hammer, *Molecular Imaging & Biology* **2009**, *11*, 167-177.
- 19) How to Improve Your Image, M. J. Therien, *Nature (London)* **2009**, *458*, 716-717.

- 20) Tunable Leuko-polymersomes that Adhere Specifically to Inflammatory Markers, G. P. Robbins, R. L. Saunders, J. B. Haun, J. Rawson, M. J. Therien, and D. A. Hammer, *Langmuir* **2010**, *26*, 14089–14096.
- 21) A Generalized System for Photo-Responsive Membrane Rupture in Polymersomes, N. P. Kamat, G. P. Robbins, J. Rawson, M. J. Therien, I. J. Dmochowski, and D. A. Hammer, *Adv. Funct. Mater.* **2010**, *20*, 2588–2596.
- 22) Effects of Membrane Rheology on Leuko-polymersome Adhesion to Inflammatory Ligands, G. P. Robbins, D. Lee, J. S. Katz, P. R. Frail, M. J. Therien, J. C. Crocker, D. A. Hammer, *Soft Matter* **2011**, *7*, 769–779.
- 23) Sensing Membrane Stress with Near IR-emissive Porphyrins, N. P. Kamat, Z. Liao, L. E. Moses, J. Rawson, M. J. Therien, I. J. Dmochowski, and D. A. Hammer, *Proc. Natl. Acad. Sci. U.S.A.* **2011**, *108*, 13984–13989.
- 24) Upconversion Luminescence and X-Ray Excited Scintillation from Single-Composition Rare-Earth Doped Yttrium Oxide Nanocrystals, I. N. Stanton, J. A. Ayres, and M. J. Therien, *Dalton Trans.* **2012**, *41*, 11576–11578.
- 25) Soft Biodegradable Polymersomes from Caprolactone-Derived Polymers, J. S. Katz, K. A. Eisenbrown, E. D. Johnston, N. P. Kamat, J. Rawson, M. J. Therien, J. A. Burdick, and D. A. Hammer, *Soft Matter*, **2012**, *37*, 10853–10862.
- 26) Biodegradable Polymersomes for the Delivery of Gemcitabine to Panc-1 Cells, N. Sood, W. T. Jenkins, X.-Y. Yang, N. N. Shah, J. S. Katz, C. J. Koch, P. R. Frail, M. J. Therien, D. A. Hammer, and S. M. Evans, *J. Pharmaceutics*, **2013**, 932797.
- 27) Aqueous Self-Assembly of Poly(ethylene oxide)-block-Poly( $\epsilon$ -caprolactone) (PEO-b-PCL) Copolymers: Disparate Diblock Copolymer Compositions Give Rise to Nano- and Meso-Scale Bilayered Vesicles, W. Qi, P. P. Ghoroghchian, G. Li, D. A. Hammer, and M. J. Therien, *Nanoscale*, **2013**, *5*, 10908–10915.
- 28) Caging Metal Ions with Visible Light-Responsive Nano-Polymersomes, J. C. Griepenburg, N. Sood, K. Vargo, D. Williams, J. Rawson, M. J. Therien, D. A. Hammer, and I. J. Dmochowski, *Langmuir* **2015**, *31*, 799–807; DOI: [10.1021/la5036689](https://doi.org/10.1021/la5036689).

**Exemplary Additional Publications over the Three Previous Years (2012-2015):**

- 1) Composite Electronic Materials Based on Poly(3,4-propylenedioxythiophene) and Highly Charged Poly(aryleneethynylene)-Wrapped Carbon Nanotubes for Supercapacitors, M. R. Rosario-Canales, P. Deria, M. J. Therien, and J. J. Santiago-Avilés, *ACS Appl. Mater. Interfaces* **2012**, *4*, 102-109.
- 2) Acentric 2-D Ensembles of D-br-A Electron-Transfer Chromophores via Vectorial Orientation within Amphiphilic n-Helix Bundle Peptides for Photovoltaic Device Applications, J. Koo, J. Park, A. Tronin, R. Zhang, V. Krishnan, J. Strzalka, I. Kuzmenko, H. C. Fry, M. J. Therien, and J. K. Blasie, *Langmuir* **2012**, *28*, 3227–3238.
- 3) Design of Coupled Porphyrin Chromophores with Unusually Large Hyperpolarizability, N. Jiang, G. Zuber, S. Keinan, A. Nayak, W. Yang, M. J. Therien, and D. N. Beratan, *J. Phys. Chem. C* **2012**, *116*, 9724–9733.
- 4) Electronic Transport in Porphyrin Supermolecule-Gold Nanoparticle Assemblies, D. Conklin, S. Nanayakkara, T.-H. Park, M. F. Lagadec, J. T. Stetcher, M. J. Therien, and D. A. Bonnell, *Nano Lett.* **2012**, *12*, 2414–2419.
- 5) Quasi-Ohmic Single Molecule Charge Transport through Highly Conjugated *meso*-to-*meso* Ethyne-Bridged Porphyrin Wires, Z. Li, T.-H. Park, J. Rawson, M. J. Therien, and E. Borguet, *Nano Lett.* **2012**, *12*, 2722–2727.
- 6) Enhanced Dispersion of CdSe/MEH-CN-PPV Hybrid Nanocomposites by in situ Polymerization using AEM as Photopolymerizable Precursor, Y. Park, J. Park, M. J. Therien, and A. D. Stiff-Roberts, *Colloid Polym. Sci.* **2012**, *290*, 1501–1509.

- 7) Effect of Solvent Polarity and Electrophilicity on Quantum Yields and Solvatochromic Shifts of Single-Walled Carbon Nanotube Photoluminescence, B. A. Larsen, P. Deria, J. M. Holt, I. N. Stanton, M. J. Heben, M. J. Therien, and J. L. Blackburn, *J. Am. Chem. Soc.* **2012**, *134*, 12485–12491.
- 8) Exploiting Plasmon Induced Hot Electrons in Molecular Electronic Devices, D. Conklin, S. Nanayakkara, T.-H. Park, M. F. Lagadec, J. T. Stetcher, X. Chen, M. J. Therien, and D. A. Bonnell, *ACS Nano*, **2013**, *7*, 4479–4486.
- 9) Raman Spectroscopic Investigation of Individual Single-Walled Carbon Nanotubes Helically Wrapped by Ionic, Semiconducting Polymers, S. Bonhommeau, P. Deria, M. G. Glesner, D. Talaga, S. Najjar, C. Belin, L. Auneau, S. Trainini, M. J. Therien, and V. Rodriguez, *J. Phys. Chem. C* **2013**, *117*, 14840–14849.
- 10) Origins of the Helical Wrapping of Phenylene-Ethynylene Polymers about Single-Walled Carbon Nanotubes, C. D. Von Bargen, C. M. MacDermaid, O.-S. Lee, P. Deria, M. J. Therien, and J. G. Saven, *J. Phys. Chem. B* **2013**, *117*, 12953–12965.
- 11) The Evolution of Spin Distribution in the Photoexcited Triplet State of Ethyne-Elaborated Porphyrins, P. J. Angiolillo, J. Rawson, P. R. Frail, and M. J. Therien, *Chem. Commun.* **2013**, *49*, 9722–9724.
- 12) Computational De Novo Design and Characterization of a Protein that Selectively Binds a Highly Hyperpolarizable Abiological Chromophore, H. C. Fry, A. Lehmann, L. E. Sinks, I. Asselberghs, A. Tronin, V. Krishnan, J. K. Blasie, K. Clays, W. F. DeGrado, J. G. Saven, and M. J. Therien, *J. Am. Chem. Soc.* **2013**, *135*, 13914–13926.
- 13) Ionic Self-Assembly Provides Dense Arrays of Individualized, Aligned Single Walled Carbon Nanotubes, J.-H. Olivier, P. Deria, J. Park, A. Kumbhar, M. Andrian-Albescu, and M. J. Therien, *Angew. Chemie.* **2013**, *52*, 13080–13085.
- 14) Single-Handed Helical Wrapping of Single-Walled Carbon Nanotubes by Chiral, Ionic, Semiconducting Polymers, P. Deria, C. D. Von Bargen, J.-H. Olivier, A. S. Kumbhar, J. G. Saven, and M. J. Therien, *J. Am. Chem. Soc.* **2013**, *135*, 16220–16234.
- 15) Fluence-Dependent Singlet Exciton Dynamics in Length-Sorted Chirality-Enriched Single-Wall Carbon Nanotubes, J. Park, P. Deria, J.-H. Olivier, and M. J. Therien, *Nano Lett.* **2014**, *14*, 504–511. DOI: [10.1021/nl403511s](https://doi.org/10.1021/nl403511s).
- 16) One-Pot Solvothermal Synthesis of Highly Emissive, Sodium-codoped, LaF<sub>3</sub> and BaLaF<sub>5</sub> Core-Shell Upconverting Nanocrystals, J. T. Stecher, A. B. Rohlfing, and M. J. Therien, *Nanomaterials* **2014**, *4*, 69–86. DOI: [10.3390/nano4010069](https://doi.org/10.3390/nano4010069).
- 17) The Biochemistry and Theory of Proton Coupled Electron Transfer, A. Migliore, N. F. Polizzi, M. J. Therien, and D. N. Beratan, *Chem. Rev.* **2014**, *114*, 3381–3465. DOI: [10.1021/cr4006654](https://doi.org/10.1021/cr4006654).
- 18) Europium- and Lithium-Doped Yttrium Oxide Nanocrystals that Provide a Linear Emissive Response with X-ray Radiation Exposure, I. N. Stanton, M. D. Belley, G. Nguyen, A. Rodrigues, Y. Li, D. G. Kirsch, T. T. Yoshizumi, and M. J. Therien, *Nanoscale* **2014**, *6*, 5284–5288. DOI: [10.1039/C4NR00497C](https://doi.org/10.1039/C4NR00497C).
- 19) Hapticity-Dependent Charge Transport through Carbodithioate-Terminated [5,15-Bis(phenylethynyl)porphinato]-zinc(II) Complexes in Metal-Molecule-Metal Junctions, Z. Li, M. Smeu, T.-H. Park, J. Rawson, Y. Xing, M. J. Therien, M. A. Ratner, and E. Borguet, *Nano Lett.* **2014**, *14*, 5493–5499. DOI: [10.1021/nl502466a](https://doi.org/10.1021/nl502466a).
- 20) Femtosecond pulse train shaping improves two-photon excited fluorescence measurements, J. K. Park, M. C. Fischer, K. Susumu, M. J. Therien, and W. S. Warren, *Opt. Lett.* **2014**, *39*, 5606–5609. DOI: [10.1364/OL.39.005606](https://doi.org/10.1364/OL.39.005606).
- 21) Potentiometric, Electronic, and Transient Absorptive Spectroscopic Properties of Oxidized Single-Walled Carbon Nanotubes Helically Wrapped by Ionic, Semiconducting Polymers in Aqueous and Organic Media, P. Deria, J.-H. Olivier, J. Park, and M. J. Therien, *J. Am. Chem. Soc.* **2014**, *136*, 14193–14199. DOI: [10.1021/ja507457z](https://doi.org/10.1021/ja507457z).

- 22) Tailoring Porphyrin-based Electron Accepting Materials for Organic Photovoltaics, J. Rawson, A. C. Stuart, W. You, and M. J. Therien, *J. Am. Chem. Soc.* **2014**, *136*, 17561–17569. DOI: [10.1021/ja5097418](https://doi.org/10.1021/ja5097418).
- 23) Design of Diethynyl Porphyrin Derivatives with High NIR Fluorescence Quantum Yields, K. Susumu and M. J. Therien, *J. Porphyrins Phthalocyanines*. **2015**, *19*, 205–218. DOI: [10.1142/S1088424614501107](https://doi.org/10.1142/S1088424614501107).
- 24) Use of a Real-Time Fiber-Optic Detector for the Measurement of Absolute Dose Rate in MRT with Sub-Millimeter Resolution, M. D. Belley, I. N. Stanton, M. Hadsell, R. Ger, B. W. Langloss, J. Lu, O. Zhou, S. X. Chang, M. J. Therien, and T. T. Yoshizumi, *Med. Phys.* **2015**, *42*, 1966-1972; DOI: [10.1118/1.4915078](https://doi.org/10.1118/1.4915078).
- 25) Electron Spin Relaxation of Hole and Electron Polarons in  $\pi$ -Conjugated Porphyrin Arrays: Spintronic Implications, J. Rawson, P. J. Angiolillo, P. R. Frail, I. Goodenough, and M. J. Therien, *J. Phys. Chem. B*. **2015**, *119*, DOI: [10.1021/jp5122728](https://doi.org/10.1021/jp5122728).
- 26) Single-Step Assembly of Multi-Modal Imaging Nanocarriers: MRI and Long-Wavelength Fluorescence Imaging, N. M. Pinkerton, M. E. Gindy, V. L. Calero-DdelC, T. Wolfson, R. F. Pagels, D. Adler, D. Gao, S. Li, R. Wang, M. Zevon, N. Yao, C. Pacheco, M. J. Therien, C. Rinaldi, P. J. Sinko, R. K. Prud'homme *Adv. Healthcare Mater.* **2015**, *4*, DOI: [10.1002/adhm.201400766](https://doi.org/10.1002/adhm.201400766).
- 27) Unambiguous Diagnosis of Photoinduced Charged Carrier Signatures in a Stoichiometrically Controlled Semiconducting Polymer-Wrapped Carbon Nanotube Assembly, J.-H. Olivier, J. Park, P. Deria, J. Rawson, Y. Bai, A. Kumbhar, and M. J. Therien, *Angew. Chem., Int. Ed. Engl.* **2015**, *55*, DOI: [10.1002/anie.201501364](https://doi.org/10.1002/anie.201501364).
- 28) Near Infrared-to-Visible Photon Upconversion Enabled by Highly Conjugated Sensitizers under Low-Power Noncoherent Illumination, J.-H. Olivier, Y. Bai, H. Uh, H. Yoo, M. J. Therien, and F. N. Castellano, *J. Phys. Chem. A* **2015**, *119*, 5642–5649. DOI: [10.1021/acs.jpca.5b03199](https://doi.org/10.1021/acs.jpca.5b03199).

**ACTIVE OTHER SUPPORT (changes from previous submission have been highlighted)**

**Michael J. Therien**

**Title and Agency ID#:** Charge-Transfer Dynamics Relevant to Protein-Mediated Energy Transduction  
R01-GM071628 (Therien's Role: PI)

**Time Commitment:** 0.67 summer month per year

**Supporting Agency:** National Institutes of Health

**Name and address of the Funding Agency's Procuring Contracting/Grants Officer:**

Dr. Ward W. Smith

National Institute of General Medical Sciences, Building 45, Room 2As-19F, MSC 6200, 45 Center Drive  
Bethesda, MD 20892-6200

**Performance Period:** 09/01/2011-01/31/2016 (End date changed due to no cost extension)

**Total Award Amount for this PI for Performance Period:**

**Location(s) of Research:** Duke University

**Brief description of project's goals:** The goals of this project are to probe mechanistic issues germane to proton-coupled electron-transfer reactions and hole hopping processes in de novo designed protein environments, and examines models of macromolecular hole transfer (HT) near the tunneling/multi-step hopping transition point.

**Specific Aims:**

1. Interrogate single-step electron and hole transfer dynamics in de novo tetra- $\alpha$ -helical protein assemblies containing D-Sp-A cofactors utilizing modern experimental and theoretical methods;
2. Design, characterize and measure multi-step charge migration dynamics in de novo hole transfer proteins with protein-based pathways.

**There is no overlap with the current project.**

**Title and Agency ID#:** UNC EFRC: Center for Solar Fuels Phase I  
DE-SC0001011, (Therien's Role: Co-PI)

**Time Commitment:** 0.5 summer month per year

**Supporting Agency:** University of North Carolina at Chapel Hill (Prime: Department of Energy, Office of Basic Energy Sciences, EFRC Program Grant (Energy Frontier Research Center).

**Name and address of the Funding Agency's Procuring Contracting/Grants Officer:**

Dr. Jeffrey Krause and Dr. B Gail McLean

Office of Basic Energy Sciences, SC-22.1/Germantown Building, U.S. Department of Energy, 1000  
Independence Avenue, SW Washington, D.C. 20585-1290

**Performance Period:** 08/01/2009-07/31/2014 (Project closed)

**Total Award Amount for this PI for Performance Period:**

**Location(s) of Research:** Duke University

**Brief description of project's goals and specific aims:** The goal of this project is to exploit molecular and nanoscale structures, polymeric materials, and modern spectroscopic methods to design devices that provide for light-driven generation of solar fuels.

**There is no overlap with the current project.**

**Title and Agency ID#:** Organic, Nanoscale, & Self-Assembled Structures Relevant to Solar Energy Conversion  
DE-SC0001517 (Therien's Role: PI)

**Time Commitment:** 0.61 summer month per year

**Supporting Agency:** Department of Energy

**Name and address of the Funding Agency's Procuring Contracting/Grants Officer:**

Dr. Mark T. Spitler

Office of Basic Energy Sciences, SC-22.1/Germantown Building, U.S. Department of Energy, 1000 Independence Avenue, SW, Washington, D.C. 20585-1290

**Performance Period:** 09/01/2012-02/28/2016 (End date changed due to no cost extension)

**Total Award Amount for this PI for Performance Period:**

**Location(s) of Research:** Duke University

**Brief description of project's goals:** The goals of this project are to elucidate the molecular-level principles by which complex chemical systems carry out photochemical charge separation, transport, and storage that will ultimately impact the design of practical solar energy conversion and storage devices.

**Specific Aims:**

1. Delineate new compositions of matter relevant to solar energy conversion;
2. Understand the basic photophysical properties of next-generation conjugated materials for excitonic solar cells;
3. Elucidate rules and principles that govern charge transfer, charge migration, photoconductivity, the extent of charge and exciton delocalization, and exciton diffusion dynamics in structures and assemblies relevant to light-driven energy transduction;
4. Probe and modulate the extent of electronic coupling between conjugated organic materials and nanoscale structures in both ground and excited states;
5. Engineer high quantum yield electron-hole pair production from initially prepared excitonic states in organic materials and organic compositions that feature nanoscale, electrooptically active components.

**There is no overlap with the current project.**

**Title and Agency ID#:** Collaborative Research: ARI-MA: Nuclear Data Measurements Using Gamma Rays and Radiation Detector Development

2012-DN-077-ARI062-03 (Therien's Role: Co-PI)

**Time Commitment:** 0.25 summer month per year

**Supporting Agency:** Department of Homeland Security

**Name and address of the Funding Agency's Procuring Contracting/Grants Officer:**

Shareef Prater

U.S. Department of Homeland Security, Mail Stop 0115, 245 Murray Lane, SW, Room 3051, Washington, DC 20528-0115

**Performance Period:** 09/15/2012-09/14/2016

**Total Award Amount for this PI for Performance Period:**

**Location(s) of Research:** Duke University

**Brief description of project's goals and specific aims:** The goals of this project are to acquire data for nuclear forensics and  $\gamma$ -ray beam interrogation technologies, and nanoparticle-based scintillator development for  $\gamma$ -ray and neutron detection.

**There is no overlap with the current project.**

**Title and Agency ID#:** NSEC on Molecular Function at the Nano-Bio Interface

553113 (Prime: NSF DMR08-32802) (Therien's Role: Co-PI)

**Time Commitment:** 0.3 summer month per year

**Supporting Agency:** University of Pennsylvania, (Prime: NSF NSEC)

**Name and address of the Funding Agency's Procuring Contracting/Grants Officer:**

Dr. David A. Brant

National Science Foundation, 4201 Wilson Blvd, Rm 1065N, Arlington, VA 22230

**Performance Period:** 09/01/2009-08/31/2014 (Project closed)

**Total Award Amount for this PI for Performance Period:**

**Location(s) of Research:** Duke University

**Brief description of project's goals and specific aims:** The goal of this project is to build novel biomaterials that possess optoelectronic function at nonbiological interfaces.

**There is no overlap with the current project.**

**Title and Agency ID#:** Development of a Novel Method to Detect Prostate Cancer Circulating Tumor Cells (CTCs) Based on Epithelial Mesenchymal Transition Biology

W81XWH-12-1-0253 – PC110452 (Therien's Role: Co-PI)

**Time Commitment:** 0.09 summer month per year

**Supporting Agency:** Department of Defense/USAMRAA

**Name and address of the Funding Agency's Procuring Contracting/Grants Officer:**

Amber Stillrich

U.S. Army Medical Research Acquisition Activity, 820 Chandler Street, Fort Detrick, MD 21702-5014

**Performance Period:** 09/10/2012-09/09/2015 (End date changed due to no cost extension)

**Total Award Amount for this PI for Performance Period:**

**Location(s) of Research:** Duke University

**Brief description of project's goals:** The goal of this project is to develop a novel circulating tumor cell capture technology based on epithelial-mesenchymal transition biology and nanoparticle near-infrared emissive polymersomes (NIR-EPs).

**Specific Aims:**

1. Develop and optimize a novel polymersome-based CTC capture method using NIR-EPs bearing conjugated antibodies to EpCAM, N and O-cadherins, and PSMA;
2. Assemble circulating tumor cell capture using novel antibody-targeted NIR-EPs in men with mCRPC.

**There is no overlap with the current project.**

**Title and Agency ID#:** Frequency Upconversion for Enhanced Light-Harvesting in Solar Photoconversion XEV-2-22202-01 (Prime: DE-AC36-08GO28308) (Therien's Role: Co-PI)

**Time Commitment:** 0.0 summer month per year

**Supporting Agency:** Department of Energy, NREL

**Name and address of the Funding Agency's Procuring Contracting/Grants Officer:**

Dr. Andrew Ferguson

National Renewable Energy Laboratory, 15013 Denver West Parkway, Golden, CO 80401, 303-275-3000

**Performance Period:** 02/13/2012-02/12/2014 (Project closed)

**Total Award Amount for this PI for Performance Period:**

**Location(s) of Research:** Duke University

**Brief description of project's goals and specific aims:** The goal of this project is to develop solar conversion devices via a strategy that decouples photon collection from photocurrent generation through systems that can convert low-energy (red-to-near-infrared [NIR]) photons to higher-energy (visible) photons in conjunction with existing PV platforms, thereby enabling a substantial increase in photocurrent while maintaining a high open-circuit voltage.

**There is no overlap with the current project.**

**Title and Agency ID#:** Circumventing Therapeutic Resistance and the Emergence of Disseminated Breast Cancer Cells through Non-Invasive Optical Imaging

W81XWH-13-1-0086 (Therien's Role: PI)

**Time Commitment:** 0.67 summer month per year

**Supporting Agency:** Department of Defense/USAMRAA

**Name and address of the Funding Agency's Procuring Contracting/Grants Officer:**

Dr. Dan Monson

Congressionally Directed Medical Research Programs (CDMRP), 1077 Patchel Street, Fort Detrick, MD 21702

**Performance Period:** 07/01/2013-06/30/2016

**Total Award Amount for this PI for Performance Period:**

**Location(s) of Research:** Duke University

**Brief description of project's goals:** The goal of this project is to create a highly sensitive non-invasive imaging modality to characterize the molecular profile of all breast cancer sites of disease, including micrometastases.

**Specific Aims:**

1. Profile a panel of molecularly heterogeneous human breast cancer cell lines using cocktails of antibody-conjugated NIREPs;
2. To phenotype primary and metastatic sites of breast cancer using targeting NIR-emissive polymersomes and determine their response to targeted therapies.

**This is the current project.**

**Title and Agency ID#:** Collaborative Research: De novo Protein Constructs for Photosynthetic Energy Transduction (Therien's Role: PI)

**Time Commitment:** 0.93 summer month per year

**Supporting Agency:** National Science Foundation

**Name and address of the Funding Agency's Procuring Contracting/Grants Officer:**

Dr. David A. Rockcliffe

National Science Foundation, 4201 Wilson Blvd, Rm 655S, Arlington, VA 22230

**Performance Period:** 08/15/2014-07/31/2017

**Total Award Amount for this PI for Performance Period:**

**Location(s) of Research:** Duke University

**Brief description of project's goals and specific aims:** The goal of this project is to exploit de novo protein design to understand the essential design principles of photosynthetic energy transduction and storage. An integrated, multi-disciplinary approach is employed toward this goal, and focuses on the evolution of peptide-cofactor complexes that undergo photoinduced charge-transfer reactions, where the protein matrix stabilizes the charge-separated state and guides the efficient separation of electrons and holes.

**There is no overlap with the current project.**

**This is a new active project.**

**Title and Agency ID#:** Real Time, In-Vivo, Radiation Dose Monitoring for External Beam Radiation Therapy and Brachytherapy (Therien's Role: PI)

**Time Commitment:** 0.6 summer month per year

**Supporting Agency:** Duke Coulter Translational Partnership

**Name and address of the Funding Agency's Procuring Contracting/Grants Officer:**

Dr. Barry Myers

Department of Biomedical Engineering, Duke University, Pratt School of Engineering, Durham, NC 27708

**Performance Period:** 09/01/2014-08/31/2015

**Total Award Amount for this PI for Performance Period:**

**Location(s) of Research:** Duke University

**Brief description of project's goals and specific aims:** This project focuses on further development of the NS-FOD (nano-scintillator fiber optic dosimeter), a device based on nanoscale scintillating materials that provides accurate, pinpoint, and real-time radiation dosimetry for clinical brachytherapy (implanted radiation), external beam radiation, electron therapy, IMRT (intensity modulated radiation therapy), and VMAT (volumetric modulated arc therapy) applications.

**There is no overlap with the current project.**

**This is a new active project.**